ChemComm

HIGHLIGHT

View Article Online
View Journal | View Issue

Cite this: *Chem. Commun.*, 2025, **61**, 2858

Biointerface engineering of flexible and wearable electronics

Alebel Nibret Belay, [ab] Rui Guo,*[a] Payam Ahmadian Koudakan [a] and Shuaijun Pan *[ac]

Biointerface sensing is a cutting-edge interdisciplinary field that merges conceptual and practical aspects. Wearable bioelectronics enable efficient interaction and close contact with biological components such as tissues and organs, paving the way for a wide range of medical applications, including personal health monitoring and medical intervention. To be applicable in real-world settings, the patches must be stable and adhere to the skin without causing discomfort or allergies in both wet and dry conditions, as well as other desirable features such as being ultra-soft, thin, flexible, and stretchable. Biosensors have emerged as promising tools primarily used to directly detect biological and electrophysiological signals, enhancing the efficacy of personalized medical treatments and enabling accurate tracking of human well-being. This review highlights the engineering of skin-tissue surfaces/interfaces and their interactions with wearable patches, aiming for both a broad and in-depth understanding of the mechanical and physicochemical properties required for the advancement of flexible and wearable skin patches. Specifically, the advantages of flexible bioelectronics and sensors with optimized surface geometry for long-term diagnosis are discussed. This insight aims to guide the future development of functional materials that can interact with human tissue in a controlled manner. Finally, we provide perspectives on the challenges and potential applications of biointerface engineering in wearable devices.

Received 15th November 2024,
Accepted 9th January 2025

DOI: 10.1039/d4cc06078d

rsc.li/chemcomm

1. Introduction

Biointerface engineering is an interdisciplinary field that focuses on designing, developing, and manipulating the interfaces between biological systems and materials or devices.[1–3] The growing popularity of wearable technology has sparked widespread public interest and has substantially impacted society and the economy, transforming personal lifestyles and the healthcare environment.[4–6] Specifically, bioelectric devices have emerged as a new paradigm for various medical applications such as medical devices, bioelectric devices, sensors, drug delivery systems, tissue engineering, molecular engineering, biosensors, *etc.*[7–11] However, most stretchable electronic materials and devices still have elastic

[a] *College of Chemistry and Chemical Engineering, Hunan University, Changsha 410082, China. E-mail: rguo@hnu.edu.cn, pansj@hnu.edu.cn*
[b] *Department of Chemistry, College of Science, Bahir Dar University, P.O. Box 79, Bahir Dar, Ethiopia*
[c] *Department of Chemical Engineering, University of Melbourne, Parkville 3010, Australia*

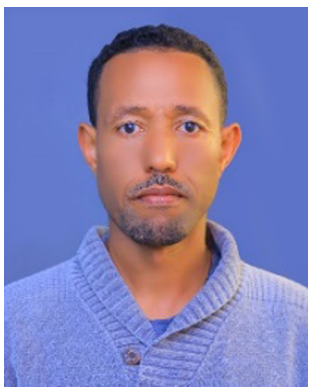

Alebel Nibret Belay

Dr Alebel N. Belay is an assistant professor at Bahir Dar University, Ethiopia. He received his PhD from the University of the Free State, South Africa, and is currently a postdoc researcher in the College of Chemistry and Chemical Engineering at Hunan University, China. His research interest focuses on bio-sensing materials.

Rui Guo

Dr Rui Guo is a researcher in the College of Chemistry and Chemical Engineering at Hunan University, China. She received her doctoral degree of chemical engineering from Hunan University. Her research surrounds coatings, thin films, and electrochemical process engineering.

moduli orders of magnitude higher than soft biological tissues, limiting their applicability and long-term biocompatibility.[8] Flexible and stretchable skin sensors are an important category within bioelectrical devices that capture biophysiological signals and analyze biomolecules directly on the human body. In this context, biointerface sensors make contact with appropriate human body sites to extract precise information and intervene by providing electrical stimulation or a visible signal. Furthermore, the potential applications of biointerface electronics that continuously and seamlessly interact with the body could be further extended into neurology, real-time health monitoring, diagnosis, and treatments.[12–14]

Bioelectronic components are traditionally developed in rigid and flat forms, and current systems do not guarantee effective integration with dynamic surfaces, such as the skin's texture, curves, and movements. For instance, to achieve maximum performance, bioadhesive materials must exhibit low modulus, high electrical stability, and optimal stimulation functions.

However, the precise engineering of bioelectronic devices to create adaptable and conformable electrode–skin interfaces remains challenging such as poor contact, limited biocompatibility, unstable fixation, tissue irritation/scar formation, and uncontrolled mechanical buckling.[15–19] As a result, skin–device interfaces often require customized shapes, enhanced stability, and good electrical conductivity, which frequently rely on physical fixation or surgical sutures.

Fig. 1 illustrates three types of bioelectrode interfaces based on their physical interaction with targeted body parts: non-invasive, semi-invasive (or minimally invasive), and invasive (Table 1). (i) A non-invasive biointerface is external to the body, making it suitable for analyzing naturally excreted biomarkers (*e.g.*, fluids and gases). Examples of wearable electronic devices involving non-invasive biointerface include sweat-sensing tools,[5] dental implants monitoring saliva,[6] tear-tracking contact lens sensors,[7] and ingestible electronics.[9] (ii) A semi-invasive biointerface bridges the gap between the non-invasive and invasive modalities by positioning the sensor outside the body while inserting the probe inside to sample extracellular fluid.[10,11] (iii) Invasive biointerfaces are placed inside the body (implanted) and come into close contact with blood, extracellular fluid, or

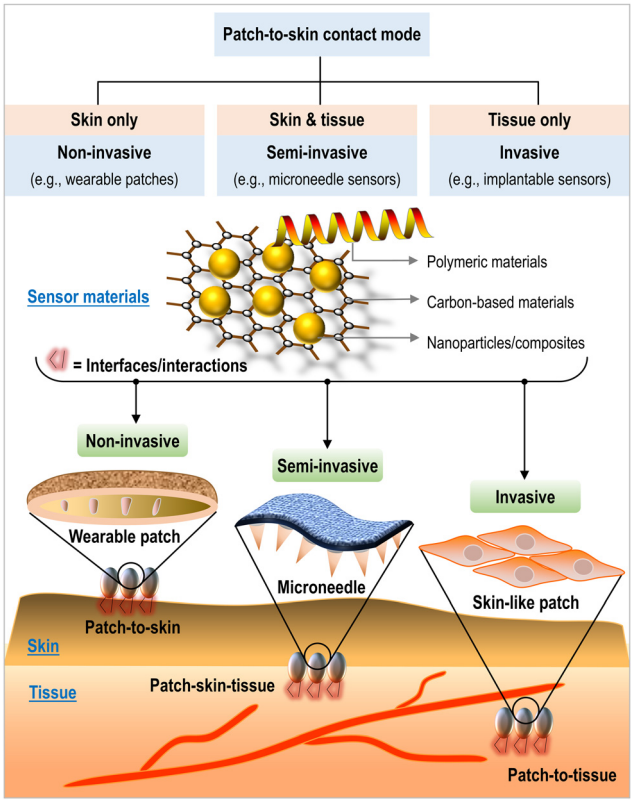

Fig. 1 Biointerface classification based on patch-to-skin interactions.

specific organs. In invasive cases, the close contact between the sensor and tissue often produces a more sensitive signal because the concentration of the biomarker or stimulus is higher near the tissue surface.

The foreign body response, consisting of macrophages and their giant cells, is the final stage of inflammation and wound healing after implantation of a medical device, prosthesis, or biological material. Foreign body reactions and biocompatibility issues hinder long-term operation and accurate detection.[23,24] Among the listed three types of biointerfaces, the non-invasive biointerface is generally recognized as safe, needle-free, infection-free, and painless. It offers the advantage of targeting

Payam Ahmadian Koudakan

Dr Payam A. Koudakan is a postdoctoral fellow in the College of Chemistry and Chemical Engineering at Hunan University, China. He earned a PhD in Chemistry from the University of Science and Technology of China. His research interest is developing electrode materials for applications in catalysis, batteries, and sensors.

Shuaijun Pan

Dr Shuaijun Pan is a professor of chemistry and chemical engineering at Hunan University, funded by the National Natural Science Foundation of China, and an Honorary Fellow at the University of Melbourne, Australia. His research focuses on polymers, surfaces, and interfaces for applications in self-cleaning, catalysis, and energy storage and conversions.

Table 1 Comparison of non-invasive, semi-invasive, and invasive detections

Performance	Non-invasive	Semi-invasive	Invasive	Ref.
Procedure	Best suited for routine diagnostic, monitoring, or certain therapeutic	Moderate for a variety of treatments where traditional surgery is not necessary	Complex, typically used when non-invasive or semi-invasive options are not sufficient	5 and 20
Safety	Very high, lower risk of complications (*e.g.*, infection, bleeding, long recovery)	High, but slightly higher risk than non-invasive and lower risk than invasive	Low with higher risk of complications, but advancements in surgical techniques and post-operative care have reduced risks	5 and 19
Comfort	Very high, due to lack of physical trauma	High, less pain and faster recovery than invasive	Low, due to pain, complications, and longer recovery time	21 and 22
Effectiveness	Effective for diagnosis, monitoring, and certain therapeutic interventions	Effective for many conditions (*e.g.*, tumors, organ repair), with targeted treatment	Highly effective for complex or large conditions (*e.g.*, large tumors, organ failures)	21 and 22
Recovery time	None, don't involve physical interventions	Faster, due to smaller incisions and less tissue damage	Longer, due to major incisions and greater tissue disruption	19
Cost	Low, but can vary with technology	Mid-range, more expensive than non-invasive	High, due to the complexity of the procedure, hospital stay, and recovery	10 and 11
Limitations	Not suitable for all conditions (*e.g.*, wet) and may not provide detailed information for some conditions (*e.g.*, biopsy or surgery)	Limited by type and severity of condition, some may require conversion to open surgery.	Larger incisions, longer recovery, and higher risks of complications like infections, blood clots, or anaesthesia-related issues	11 and 22

physiological signals such as temperature,[25] pressure,[26] strain,[27] pH,[28] and so on, as well as biochemical signals like blood glucose levels,[29] saliva,[30] interstitial fluid,[31] and sweat.[32] Additionally, non-invasive biointerfaces allow for the detection of electrophysiological signals such as electroencephalograms,[33] electrocorticograms,[34] electrocardiograms,[35] electromyograms,[36] radio waves,[37] ultrasound,[38] optoelectronic signals,[39] galvanic skin response,[40] seismocardiograms,[41] and electrochemical processes,[42] facilitating disease prevention, diagnosis, and treatment.

Overall, advancing biointerface technology requires understanding the nature and principles of the human skin–electrode interface, including technical engineering considerations for various biomedical applications.[43] Recent reports show that bioelectronics has progressed significantly from conventional rigid and rectangular shapes to ultra-soft, thin, light, flexible, stretchable, and intricately designed structures.[44–47] This transition reduces mechanical incompatibility at the device–skin interface, developing more precise and comfortable sensors and stimulators. Information obtained from the electrode–skin interface reveals details about both the inside and outside of the human body, suggesting that advanced sensing and stimulation technologies in medical diagnosis and treatments represent the future.[19,48,49] Moreover, there is a growing interest in materials and devices capable of converting mechanical energy into visible patterns or signals through luminescence. Such developments have significant implications for emerging sectors such as human–machine interfaces (artificial intelligence) and the Internet of Things (wireless sensors).[50–52]

This review systematically highlights recent advances in the interactions between wearable patches and skin interfaces, focusing on material and skin properties, including position, mounting, size, morphology, adhesion, friction, and biocompatibility. Finally, we outline the challenges and opportunities that will guide further developments in biointerface technology.

2. Nano-engineered wearable skin–patch interfaces

The success of surface modification of wearable devices with soft functional materials depends on several factors, including size, shape, dispersion, concentration, temperature, mass barrier properties, and the stress transfer performance of the device. The synthesis techniques utilized have an impact on factors like agglomeration. The use of highly conductive and printable materials in developing bioelectronic devices has resulted in flexible and stretchable designs, opening intriguing avenues for advancing manufacturing techniques.[53,54] Applying nanoscale platforms with precise sizes, geometries, surface functionalities, *etc.*, offers significant potential for developing non-invasive sensing devices, revolutionizing health monitoring, data storage, and disease diagnosis, including real-time feedback during therapy (Tables 2 and 3).[32] This approach seeks to develop advanced technology that comprises reliable and predictable systems with unique features that do not exist naturally.[55,56] Fig. 2 illustrates the potential source of electronic systems used in flexible and stretchable configurations. These systems may provide a promising alternative to bulky health monitoring tools, offering enhanced comfort, reduced social stigma, and improved patient compliance. This emerging field of bioelectronics includes sensors, light-emitting diodes, and other circuit components that create connections and interfaces with internal organs (*e.g.*, heart and brain) as well as other external organs like the skin or artificial skin scaffolds. Therefore, to allow real-time health monitoring, it is essential to consider factors such as biocompatibility, deformation, skin irritation/allergy, fit, and so on while maintaining the structural and functional integrity of the human physiological system. These considerations are critical for rapidly assessing tissue development, metabolic status, immune function, hormonal regulation, and other aspects of human health.[18,57,58]

Table 2 Summary of the different materials used in flexible wearable devices, the interaction between these materials and skin tissue surfaces, and the sensing methods used for health monitoring. [sEMG, ECoG, ECG, EMG, EEG, ECP, PPG, and SNR, are surface electromyography, electrocorticogram, electrocardiogram, electromyogram, electroencephalogram, echocardiography, photoplethysmography, and signal–noise-ratio]

Material used	Highlight	Conductivity	Impedance interface and/or SNR[a]	Skin matchable Young's modulus	Recording signals	Biocompatibility	Morphology	Ref.
PHH wet hydrogel film (PVA–HEDP–HPAA)	Tunable hydrogen bond network. Sensitivity (amplitude) of 0.11 mV and accuracy 100%.	High, 13.56 S m^{-1}	12.56 kΩ, 38.09 ± 1.28 dB	10–30 kPa	sEMG	Yes	—	59
PDMS–parylene hybrid (Au–MWCNTs/PEDOTS:PSS)	High sensitivity. The power for epileptic activity is 11.049 ± 4.513 μW. The ECoG potential at normal status is 123 ± 23 μV.	High	20.68 ± 6.65 kΩ	—	ECoG	Yes	Nanotube	60
PAAc–DES gel	High adhesion to the skin, ∼100 N m^{-1}. Excellent stretchability, >1000%. Good anti-drying and anti-freezing properties.	High, 1.26 mS cm^{-1}	Low	∼20 kPa	sEMG	Yes	—	61
Au–PDMS/rGO/PVA/(PAA–NHS) hydrogel	Robust (interfacial toughness >400 J m^{-2}). Fast adhesion formation within 5 seconds. Have the capability to be easily integrated into a wide range of wet and dynamic tissues in a detachable manner.	High, >2.6 S m^{-1}	<50 Ω	293 kPa	ECG	Yes	Nanosheet	4
PTG thin film (PEDOT:PSS/(SDS + BSL)/graphene/Cu foil)	Strong π–π interaction. Able to conformably adhere to skin. ∼100 nm ultra-thin dry epidermal electrode. Sheet resistance (R_{sh}) is ∼24 Ω sq^{-1}.	4.142 mS cm^{-1}	∼32 kΩ, 23 ± 0.7 dB	640 kPa	EOG, sEMG, ECG	Yes	Nanosheet	62
PWS film (PEDOT:PSS/WPU/D-sorbitol)	High stretchable and adhesive onto smooth skin, hairy rough skin, and wet deformable skin. The adhesive force of PWS film on the wet and dry skin are 0.43 and 0.56 N cm^{-1}, respectively.	72–545 S cm^{-1}	82 kΩ	0.21–0.33 GPa	ECG, EMG, EEG	Yes	—	63
SHE (Au–Cr–PI/PDMS/Solaris/Ecoflex/Ecoflex GEL)	Long-range wireless connectivity (up to 15 m). SHE is naturally adhering to the skin and is flexible enough to stretch and bend.	High	2.5–23 dB	7.85–125 kPa	ECG	Yes	Thin film (nanosheet)	64
bi-HEB(PANI/GOx/PtNP/NPC@MXene/Au)	Exhibits a remarkable sensitivity of 100.85 μA mm^{-1} cm^{-2} within the physiological range of 0.003–1.5 mm. High chemical stability. Strong π–π interaction.	High	35.2 ± 2.70–310.5 ± 34 kΩ, 10 ± 6–27 ± 5 dB	—	ECG, EMG, EEG, pH, tempe., glucose.	Yes	Nanoporous	65
LME electrode (LIG/MXene-$Ti_3C_2T_x$@EDOT)	Exhibits a high sensitivity to strain (2075; >22% strain) and a favorable temperature coefficient of resistance (0.52% K^{-1}). The self-alignment of EDOT oligomers is facilitated by hydrogen bonding between the anion and the electrode surface. Exhibited good stability over 20 000 cycles.	High	50.8 kΩ, 20.14 dB	—	ECG, strain, tempe.	Yes	Nanosheets	66
GCF-Opse electrode (GCF/rGO/PDMS)	Able to conformably adhere to skin in both wet and dry conditions. Water-resistant, enabling self-cleaning. Exhibits sensitive responses with a low limit of detection.	∼160 S m^{-1}	—	∼26 MPa	ECG	Yes	Nanofibers	67
AgNWs/PEDOT:PSS	Moldable and transferable thin films with dimensions <25 μm. Electromechanically stable even when subjected to bending and stretching, durable performance.	∼93 S cm^{-1}	62.76 kΩ, 12.3 dB	8.8 MPa	ECG, EMG	Yes	Nanowires	68

Table 3 Summary of different selected fabrications of wearable patches that interface non-invasively with the skin and are used to detect electrophysiological signals

Materials used	Crosslinking agent/stabilizer	Synthesis method	Advantage	Limitations/suggestions	Physiological signal/test	Ref.
Binodal EES (PDMS/[EMIM][$EtSO_4$]/Cu-foil)	[EMIM][$EtSO_4$]	Combination of semiconductor processing steps, lamination procedures, transfer printing processes, and chip placement and solder bonding.	Enable wireless power transfer, low-noise sensing, and high-speed data communication through a single radio-frequency link minimally affecting biological tissues. Implementing efficient algorithms on sensor platforms for real-time data analytics, signal processing, and dynamic baseline modulation. Synchronizing wireless data streaming from two separate devices. Designing systems that enable visual inspection of the skin interface, biocompatible while allowing neonate-friendly magnetic resonance imaging and X-ray imaging.	With additional clinical validation and testing, this technology has the potential to be widely adopted in both high- and low-resource settings. In addition, additives like ionic liquids [EMIM][$EtSO_4$] are toxic, and cannot be used for epidermal biopotential measurement.	ECG, PPG	69
CPAMC/PCA Janus hydrogel	PEGDA and BAC	Interfacial *in situ* copolymerization.	Reversible and asymmetric adhesive properties allow for stimuli-triggered non-invasively detachment on demand for myocardial infarction repair and anti-tissue-synechia. The adhesion displayed a molecularly encoded feature that mimicked the self-protective stress–strain effect found in biological tissues, leading to adaptive stiffening.	To fully utilize its potential in adjusting electrophysiology in cardiac tissue, the electrical conductivity of the CPAMC/PCA hydrogel needs improvement to better match that of native cardiac tissue.	ECP	70
SACPs (SMS/PVA/PEDOT:PSS)	Glutaraldehyde (GA)	Multi-solution processing (*i.e.*, drop-casting, spin-coating, microfluid molding, and even transfer printing).	Exhibit excellent mechanical flexibility (including low modulus, low residual strain, and high stretchability), high conductivity, and robust interface adhesion strength.	The current SACP demonstrates favorable electrical properties (up to 37 S cm^{-1}), but further enhancement and improvement of its capacity are required.	EMG	16
CuAuNW	DEHA and Na_2SO_3	Wet chemical synthesis.	With outstanding thermal and chemical stability, and moderate biocompatibility. The system is not prone to oxidation issues.	Physical incompatibility, thus causing discomfort for the user and resulting in the formation of scar tissue.	EMG, ECG	36
Epidermal electronic system (EES)		Cut-and-paste method, flexible printed circuit board process	Lies in its capability for mobile healthcare (*i.e.*, by eliminating the interference caused by lengthy epidermal interconnects). The data acquisition becomes portable.	To enhance the overall robustness of the system, it needs a self-adhesive hydrogel to enhance the adhesion strength between EES and the skin, particularly in sweating.	ECG	35 and 45
PEDOT/PSS/SA/PAM	MBAA and $CaSO_4$	*In situ* copolymerization.	Excellent durability, good robustness, strong bonding to the substrate, low impedance when in contact with the skin, easy setup, reusable properties, and the capability to acquire long-term EEG signals.	It needs improvement in the water retention capacity of the conductive hydrogel material used, for proper hydration at the interface between the electrode and the skin is crucial for minimizing impedance.	EEG	33
AgPEDOT/PSS/P3HT-NF/PVDF–HFP/EMIM–TFSI		*In situ* micro-fabrication techniques *via* the drawing process	Being less affected by sweat and more resistant to physical damage, the ability to apply electronic materials to dynamic surfaces, and immunity to motion artifacts without requiring extra hardware or computation. This provides an innovative solution to a persistent problem in the bioelectronics field.	Further improvement is needed in waterproofing, specifically for the gel electrode, to address issues such as sweat pooling or a decline in ion concentration within the gel electrolyte.	ECG	71
PTG thin film (PEDOT:PSS/(SDS–BSL)/graphene/Cu foil)	SDS and BSL	Direct chemical vapor deposition (CVD)	Ultra-conformal and dry PTG electrodes showed excellent capability of long-time and minimal motion artifact in the detection of electrophysiological signals.	It needs improvement because the gelation of PEDOT:PSS solution at high BSL concentration makes it difficult to form uniform PEDOT:PSS carrier layers by spin-coating, leading to a thick PTG film.	EOG, ECG, and sEMG	62

Table 3 (*continued*)

Materials used	Crosslinking agent/stabilizer	Synthesis method	Advantage	Limitations/suggestions	Physiological signal/test	Ref.
Au–PDMS/rGO/PVA/(PAA–NHS) hydrogel	PAA and NHS	*In situ* solution process	It can provide durable integration in wet and dynamic physiological environments. The e-bioadhesive interface's anisotropic swelling property can reduce the risk of geometric mismatch in wet physiological conditions.	The adhesion formed by the e-bioadhesive interface can be quickly reversed within 5 minutes by applying a biocompatible aqueous triggering solution.	ECG	4
PWS film (PEDOT:PSS/WPU/D-sorbitol)	D-Sorbitol	*In situ* solution process (drop-casting)	Ultra-conformal with both wet and dry skin. Ultrathin electrodes showed excellent capability of self-adhesive, long-time, and minimal motion artifact in the detection of electrophysiological signals. The biopotential signals can be resistant to motion artifacts.	It exhibits stable impedance over time when applied to dry skin, but not when exposed to sweat or moisture.	ECG, EMG, EEG	63
LME electrode (LIG/MXene-$Ti_3C_2T_x$@EDOT)	—	*In situ* polymerization self-assembly, electrophoretic deposition (EPD)	The fabrication method is simple, scalable, convenient, and cost-effective for producing high-performance multifunctional sensors. This is achieved through a single-step EPD process, without the requirement of any oxidant, allowing for easy transfer of functional materials onto an ultrathin stretchable substrate and layer-by-layer packaging.	The strain on the sensor remains below 20%. However, once the applied strain surpasses 20%, the pristine LIG loses its electrical connection entirely. This is due to the inability of LIG nanoflakes alone to sustain electrical conductivity under significant strain.	ECG, strain	72

2.1. Skin sensorial properties

Human skin is essential for perception, encompassing haptic, thermal, proprioceptive, and pain-sensing functions through the movement of ions, while also being mechanically resilient and able to self-healing for protection.[73] The mechanical properties of human tissue are important for the structure and function of the human physiological system. In Fig. 3, the electrode–skin interface represents a model of human skin as the largest organ in the body, a convenient and accessible source of information about the body's internal state through visual inspection and palpation.[74] The main function of the skin is to protect the internal organs from hazardous microbes, UV light, weather conditions, pollution, *etc.* The main function of the skin is to protect the internal organs from hazardous microbes, UV light, weather conditions, pollution, *etc.* Histological analysis revealed that the dermis, which lies between the exterior epidermis and the interior subcutaneous tissue (Fig. 3a and b), spans a large area. Composed primarily of fibrous tissues like collagen, elastic fibers, and glycosaminoglycans, the dermis has sensory and protective properties thanks to nerve endings, glands, blood vessels, and hair follicles. The hair follicles act as immune sensors by releasing certain chemokines that attract immune cells in response to mild physical stress, such as scratching.[75,76] By directly collecting biosignals from the skin, the potential for convenient and adaptive non-invasive monitoring is evident.

The skin has an elastic deformation strain of 20–30%. Its elastic modulus can vary between 1.11 kPa and 57 MPa, depending on factors like age, skin location, and testing methods.[77] This unique feature makes skin an ideal flexible substrate for wearable devices, allowing them to adapt to the shape of the skin and resist deformation during frequent body movements. However, one needs to carefully consider the nature of electronics and the skin's mechanical properties.[78,79] In addition, small changes or fluctuations of patches can disrupt the skin's balance, potentially leading to misinterpretation of the signals obtained through electronic skin sensors. Skin sensors are considered less risky than implantable devices and, therefore, are categorized as non-invasive. For instance, individuals with metal allergies may experience contact dermatitis when in touch with the sensor, which can rarely lead to systemic contact dermatitis. Most on-skin electronics are made of waterproof materials, which hinder the skin's natural secretion of sweat and other fluids, leading to excessive moisture and softening of the outermost layer called the stratum corneum. Consequently, the skin's protective barrier function could be compromised, resulting in irritant contact dermatitis, which often requires device removal. Therefore, the long-term safety of the wearable device–skin interface lacks adequate scientific evidence,[55,71,80,81] highlighting the need for continued and even expanded research.

2.2. Wearable patch-to-skin iontronic interfaces

Human skin's self-healing nature and ion-sensing capability provide a promising basis for developing flexible iontronic skins (Fig. 3b). Iontronic sensors represent a novel class of soft electronics that replicate the structure of human skin and

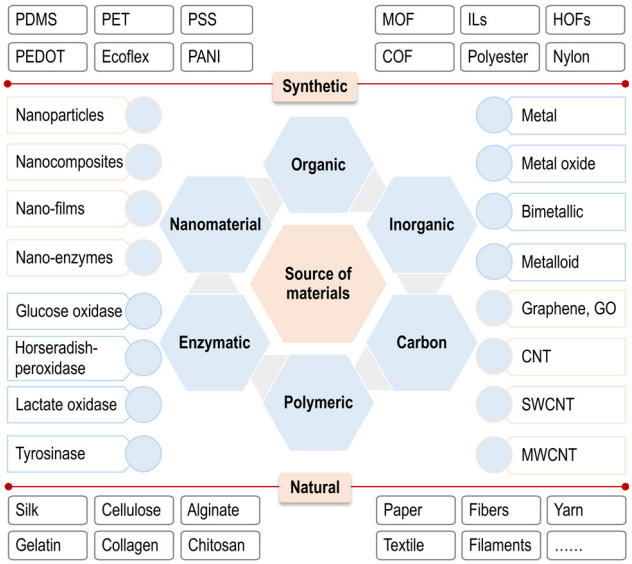

Fig. 2 Source of biochemical materials used for wearable patches. PDMS, PSS, PEDOT, PANI, MOF, ILs, HOFs, COF, GO, CNT, SWCNT, and MWCNT are polydimethylsiloxane, polystyrene sulfonate, poly(3,4-ethylene dioxythiophene), polyaniline, metal–organic frameworks, ionic liquids, hydrogen-bonded organic frameworks, covalent organic frameworks, graphene oxide, carbon nanotubes, single-walled carbon nanotubes, and multi-walled carbon nanotubes, respectively.

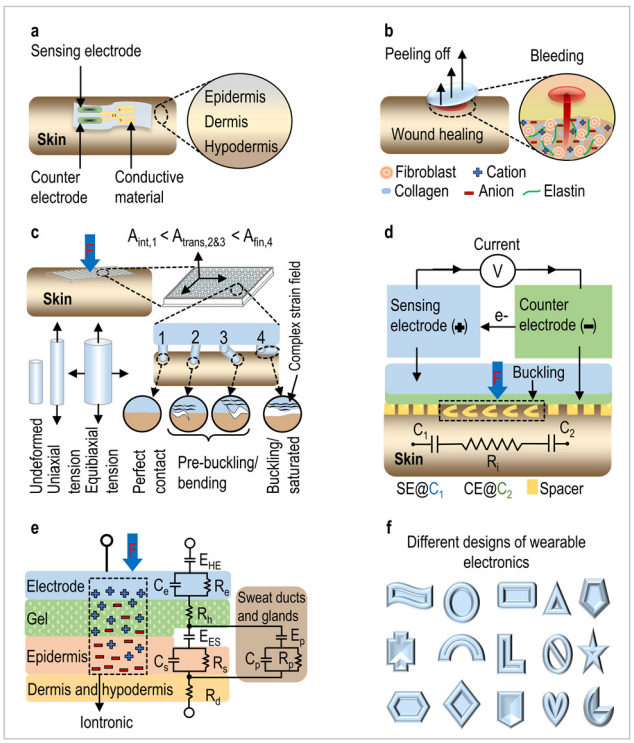

Fig. 3 Skin sensing capability and patch-to-skin iontronic interfaces. (a) Mechanosensitive electrode system contacts on arm tissue, where the skin acts as the anionic material and the counter electrode as the cationic material. (b) Skin wound healing mechanism. The inset illustrates the ion-rich nanofiber composition, showing how collagen fibers and the elastic matrix of the skin can heal with the aid of fibroblasts. (c) Mechanical terminology and material stiffness at cylindrical micropillar and skin interfaces before, during, and after the onset of buckling. (d) The effects of electrical stimulation on the skin surface and the skin–electrode interface during loading, along with a simplified equivalent circuit of the SEMS. (e) Equivalent circuit model for the skin-gel-electrode interface. E_{HE} is the half-cell potential between the hydrogel and the electrode; C_e and R_e represent the capacitance and resistance of the metal electrode; R_h is the resistance of the hydrogel; E_{ES} is the half-cell potential between the hydrogel and epidermis; C_s and R_s represent the capacitance and resistance of the epidermis; R_d is the resistance of the dermis and subcutaneous layer; E_p, C_p, and R_p represent the corresponding effect of sweat glands as a parallel conduction path through the epidermis. (f) Various forms of conductive materials used in wearing patches.

mimic its mechanical sensing functionality.[73] For bioelectronics to yield results comparable to skin, they must possess high electrical conductivity, optimal optical properties, electromagnetic and electromechanical stability, and a low elastic modulus. Researchers have prepared various conductive and stretchable synthetic materials (Fig. 2 and Tables 2, 3) to address the limitations of conventional materials utilized at biointerfaces. Specifically, polymer-based nanocomposites have been developed to measure many electrophysiological signals, thereby ensuring high-quality performance.[49,82–84] The advantage of these materials lies in the ability to fine-tune their mechanical and electrical properties according to specific needs and requirements.[68,85,86]

Zhu *et al.*[43] constructed a simple mode of iontronic sensing (skin–electrode mechanosensing structure (SEMS)) that did not require artificial ionic materials, exhibiting high-pressure resolution and spatial resolution, being capable of feeling touch and detecting weak physiological signals such as fingertip pulse under different skin humidity. They also investigated the effect of motion artifacts on the detection of pulse signals that contain motion-related frequencies that are different in the frequency domain from the characteristic pulse frequency, so that the extraction of physiological signals can be completed without interference from motion artifacts. However, a portable system may further be integrated to enable continuous monitoring of body motion or touch without affecting the subjects' daily life activities (Fig. 3a)[77,87]

Therefore, measuring the stiffness, extensibility, and mechanical strength of wearable electronics is important in evaluating patch-to-skin interfaces and tissue-engineered skin replacements.

For a material with initial length L and cross-sectional area A, a force F induces a change in dimension. Given these parameters, it is possible to calculate the stress (F/A), the strain ($\Delta l/L$, Δl represents a change in dimension), and Young's modulus of elasticity (*i.e.*, stress/strain). In this regard, a high modulus value indicates a stiff material.

Fig. 3c illustrates how a deformed pillar can exhibit different shapes during a compression test, depending on its length-to-radius aspect ratio and relative stiffness to the substrate. Additionally, capacitance in iontronic systems is directly proportional to the skin contact area at the electrode biointerface. Three contact phases are $A_{initial}$, $A_{transition}$, and A_{final}, representing the initial contact zone, transition phase, and post-instability contact zone, respectively. To analyze the deformation, the difference in the contact surface between the initial

and final states is normalized by the square of the radius (R^2). This calculation is performed using Hertz contact models around the Euler buckling load point.[88,89] The most significant change in the contact area or maximum sensitivity, occurs immediately after the initiation of buckling instability, especially when the aspect ratio is large. Specifically, the slender micropillars undergo buckling instability to maximize the change in contact area when subjected to external loads (Fig. 3c and d). A pillar with a semi-spherical end is pressed into the skin in the pre-buckling configuration. However, in the post-buckling regime, the pillar bends over with its axis parallel to the substrate, and its side area is compressed against an elastic plane. Both the pre- and post-buckling contact areas can be calculated using contact mechanics models.[90] During loading (Fig. 3d), the flexible micropillar structure (*e.g.*, polydimethylsiloxane), allows precise changes in the contact area at the skin–electrode interface, mimicking a capacitor with capacitance per unit area significantly higher than that of traditional devices. The sensing electrode in this system exhibits excellent biocompatibility and breathability, similar to a patch stuck on the skin, which can be achieved through minimal contact with the skin *via* the flexible micropillar structure.[91] The gaps between the pillars facilitate air circulation, prevent moisture build-up, and thus ensure skin dryness. Although PDMS is inherently airtight and waterproof, the counter electrode can adapt perfectly to the skin's texture, ensuring consistent iontronic capacitance throughout the interface (Fig. 3e).[92]

Furthermore, in Fig. 3d, the simple equivalent circuit of SEMS can be represented by two capacitors: C_1 for SE and C_2 for CE, C_2 is a constant and set as $\sim$100 nF cm^{-2}. These capacitors are connected in series with a resistor (R_i, *i.e.*, the resistance between the two electrodes). The entire series circuit is then connected in parallel with the coupling capacitance CE of the electrode. The recorded capacitance (C) can be approximately estimated using the formula: $1/C = (1/C_1) + (1/C_2)$. The signal output mainly depends on C_1 since C_2 remains constant, which fluctuates with the applied pressure. The distance between the two electrodes has a negligible impact on C due to the ionic nature of the skin (when we put a metal electrode in conformal contact with the skin, free electrons serve as the carriers in the electrodes while ionic fluxes contribute to the conduction in the tissue to exchange electronic and ionic signals). During the test, C decreases as the applied frequency increases. When pressure is applied, the system's micropillars bend downwards, coming into close contact with the skin and thus C is increased. A decrease in initial C or the initial contact area will increase sensitivity based on the definition of sensitivity. A spacer, a perforated polyethylene terephthalate membrane is inserted between the SE and the skin to enhance sensitivity by reducing the initial contact area, thus ensuring consistency between different devices (Fig. 3f). The impedance values between the electrodes and the skin, with and without spacers, for both SE and CE, usually range from 10^2 to 10^5 Ω in the frequency range (10^4–10^6 Hz). Once the pressure exceeds 15 kPa, the system's response becomes saturated. Therefore, the pressure-sensing electrodes are designed in two variants: one has a tunable surface microstructure to create an interface sensitive to applied pressures, while the other is firmly attached to the skin (usually, the detection limit of human skin is $\sim$100 Pa, and the response time is 30–50 ms).[93]

Xia *et al.*[94] reported a capacitive-type active wearable electronic skin, using a microgel layer as the component responsible for deformation. Electronic skins have a unique structure that generates optical and electronic signals in response to pressure changes. The electronic skin's single-layer microgel film has high-pressure sensitivity (10.1 kPa^{-1}) and low detection pressure (2 Pa), making it suitable for monitoring cardiovascular risks in a wearable mode. A protective layer of dead cells (stratum corneum) on the skin is a challenge for accurately recording physiological signals. In addition, the electrical noise caused by relative motions at the skin–electrode interfaces is a primary affecting factor of the signal quality for wearable and epidermal electronic sensors.[95] Sweat glands are another important factor, which naturally keeps skin moist due to the hydrated and porous nature of the corneum. Sweat ducts act as pumps, transporting sweat to the skin surface, where the sweat infiltrates into the porous corneum either through high pressure within the ducts or by diffusion.[55] Various ions, such as K^+, Na^+, and Cl^-, are present in sweat at concentrations around 10 mM, increasing the ionic conductivity of the corneum. Therefore, when the sensing and counter electrodes come into conformal contact with wet skin, the iontronic interface's capacity to separate electrons and ions may become higher than that of dry skin.[43] The gradual change in the baseline is due to the different states of skin hydration. The change does not hurt detecting dynamic physiological signals and touching signals. In addition, prolonged heavy sweating with high NaCl concentrations (*e.g.*, cystic fibrosis) can increase the risk of NaCl imbalance (capacitance baseline rises upon sweating).[96,97] Importantly, the spacer in the SEMS can be removed to provide a more comfortable attachment experience.

In general, ion gels and hydrogels are commonly used as ionic materials in iontronic sensing; however, ion gels are often toxic and highly absorbent, while hydrogels are prone to dehydration in the air.[98] One of the most effective approaches to address these shortcomings is to replace traditional covalently cross-linked gels with supramolecular hydrogels cross-linked by dynamic hydrogen bonds. However, they tend to over-swell and disintegrate in aqueous environments because the presence of water molecules breaks hydrogen bonds, thus further weakening their mechanical strength.[99] This instability and poor mechanical properties prevent their long-term use and implementation. So, such problems would be resolved by using phase separation methods to improve the stiffness of hydrogels and limit over-swelling by increasing the physical cross-linking density and reducing the flexibility of chain segments. Recently, researchers have developed phase-separated hydrogels that incorporate energy dissipation mechanisms such as hydrogen bonding, ionic bonding, hydrophobic association, and crystallization to enhance strength and toughness.[100,101] In addition, Xu *et al.*[102] designed a dehydration–hydration approach to transform soft and weak hydrogels into tough and recyclable supramolecular phase-separated gels using copolymerization of

sodium styrenesulfonate and sulfobetaine methacrylate in aqueous polyvinyl alcohol (PVA) solution, followed by dehydration *via* air drying and rehydration *via* swelling in water. This approach led to phase separation and the formation of domains consisting of strong polymer–polymer interactions that are critical for forming phase-separated gels.[103] Li *et al.*[104] reported a biocompatible skin–electrode interface patch for monitoring surface electromyography (sEMG) signals, incorporating a hydrogen-bonding network into a polyvinyl alcohol-based hydrogel. Specifically, hydroxyethylidene diphosphonic acid (HEDP) and 2-hydroxyphosphonoaceticacid (HPAA) were used to modify the hydrogen-bonded cross-linking network (Fig. 3e).[105,106] In this system, the hydrogen bond between the polymer chain and the HEDP molecule is disrupted due to the presence of HPAA, which releases hydroxyl groups of the polymer chains. These hydroxyl groups then interact with the skin tissue through hydrogen bonding, providing adhesion for the hydrogel.[107] $HEDPH_4$ is a tetra-acid with two pK_a values around 2–3 and the other two around 7. At a skin pH of 6–7, HEDP primarily exists as a dianion ($HEDP^{2-}$). As sweat pH rises due to changes in the concentrations of protons, sodium, and chloride ions, various strategies are employed to ensure conformal contact between the electrode and the skin. These strategies include matching the elastic modulus to promote a better fit, reducing the electrode–skin interface gap through adhesion, and improving ion and electron conduction through enhanced electrical conductivity.[4,85,108,109]

2.3. Wearable patch-to-skin haptic interfaces

Haptic feedback stimulates tactile sensations through physical stimuli (*e.g.*, vibration patterns), and plays an essential role in providing both sensory input and visual cues. The haptic interface is crucial for encoding tactile information, making it a key component in intelligent human–machine interfaces. It enables a closed-loop system where the human body can detect and respond to tactile feedback.[110,111] The development of thin and flexible materials for haptic interfaces is critical for enhancing virtual reality (VR) experiences, improving wearable devices, and advancing robotics and prosthetic technologies. However, a major challenge in using electrotactile stimulation for haptic sensing is the wide range of perceived sensation intensities. This variation is often due to changes in the impedance of the electrode–skin interface, especially when electrodes begin to peel off or when the user sweats.[112] For example, delivering haptic feedback to the hand *via* a glove-like haptic interface is frequently constrained by the bulkiness, rigid structure, and attached cables.[113] Nonetheless, electrotactile techniques provide an effective solution for minimizing the size of contact areas.[18,114] Unlike other stimulation technologies such as electromagnetic,[115] piezoelectric,[113] hydraulic,[116] or ultrasonic,[117] which rely on more complex feedback mechanisms electrotactile stimulation is simpler and more achievable. This is due to the use of thin, flexible skin-integrated electrode interfaces that apply currents directly.

Wearable electrotactile devices, such as silicone finger tubes and tattoo-like thin films, have been developed to be thin, flexible, and lightweight.[118,119] These devices can be comfortably attached to the skin without irritating.[120,121] However, the requirement for additional power sources and signal generators limits their operational range and may create a feeling of confinement. Additionally, wireless haptic interface systems face several challenges, including limited operating range due to relatively large actuators (*e.g.*, 18 mm in diameter) with significant spacing (*e.g.*, 21 mm), high power consumption, and suboptimal weight characteristics for skin mounting (*e.g.*, ~130 g in total). Furthermore, these systems lack programmable control over the intensity of haptic sensations.[93]

In the rapidly growing VR, augmented reality (AR), and mixed reality (XR) industries, genuine haptic feedback allows users to experience realistic touch sensations with objects in the virtual world (the metaverse), thus enhancing the immersive experience.[13,122,123] These interfaces provide tactile sensations that enable humans to interact with computer systems and other machines. By displaying tactile images on the skin, the enhanced VR or AR experiences go beyond what visual and auditory inputs alone can provide (Fig. 4a and b). Signals obtained from various sources, including direct graphical user interface input and wireless sensor networks (Fig. 4b), power multimodal actuators that improve the intensity and energy efficiency of haptic interactions. These interfaces can provide over extended wireless distances and offer both battery and battery-free options. Additionally, the lower packaging layer houses the electronics and exposes the actuators through octagonal openings, allowing direct contact with the skin. Such interfaces have applications for education, training, medicine, rehabilitation, gaming, entertainment, social networks, military exercises, surgery, and more.[124] Precise spatiotemporal modulation of these systems ensures resolution that meets or exceeds

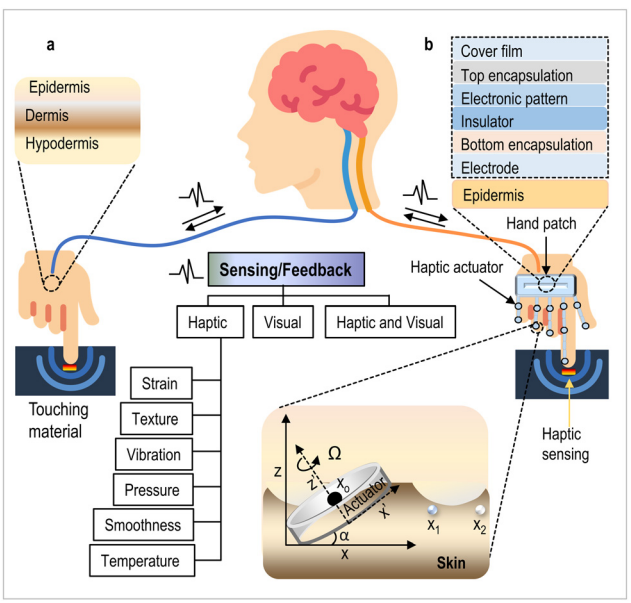

Fig. 4 Different feedback modes of human and electronic skin haptic interfaces. (a) Human skin haptic interface sensing mechanism. (b) Electronic skin haptic interface sensing mechanisms, including the cross-section of wireless electrotactile devices integrated with the skin. The inset shows the ERM actuator on the skin.

the requirements established by two-point discrimination tests, engaging skin mechanoreceptors across most body areas, except for the hands and face,[111,125] which have the highest resolution (2–4 mm). Other areas, like the upper arms, thighs, back, and abdomen, have lower resolution (~40 mm), likely due to the less dense distribution of mechanoreceptors.[126]

The direct physical interface between the eccentric rotating mass (ERM) actuator and the skin produces complex deformation patterns, resulting in enhanced sensory perception. This is a significant advancement over voice coil-type actuators. Duong *et al.*[127] introduced a slim button design that integrates multimodal audio and haptic feedback, improving the tactile interface in electronic devices. This button uses a film-type actuator made of blended relaxor ferroelectric polymers, poly(vinylidene fluoride-trifluoroethylene-chlorofluoroethylene) [P(VDF-TrFE-CFE)] and poly(vinylidene fluoride-trifluoroethylene) [P(VDF-TrFE)],[128] which generate mechanical vibrations through the fretting vibration phenomenon. The actuator delivers tactile feedback at frequencies ranging from 50 to 300 Hz and audible sounds at higher frequencies between 0.5 and 1 kHz. The lateral wave propagation across the skin is generated at an operating voltage of 3.3 V, with amplitude decreasing as the distance from the source increases. This motion is consistent with Rayleigh waves, traveling at a velocity of ~12.5 m s^{-1}. These vibrations provide sensory substitution for amputees, enabling feedback control in prosthetic robotic interfaces.[129]

Moreover, Yao *et al.*[130] introduced a soft, ultra-thin, miniaturized wireless electrotactile (WeTac) system, which delivers electrical currents through the hand to create tactile sensations, serving as an integrated tactile interface. WeTac features a dense array of tactile pixels across the hand, allowing for both tactile stimulation and accurate measurement of users' sensation thresholds. This system synchronizes with VR, AR, and robotic systems *via* Bluetooth low-energy wireless communication,[111,113] allowing users to experience tailored tactile feedback when interacting with virtual objects.[131,132] Thus, the WeTac system enables highly precise reproduction of virtual or remote touch experiences, expanding the potential for immersive applications.

2.4. Skin-mountable electronic material systems

Skin-inspired electronic materials are developed with new functionalities to address the limitations of electronic materials for bio-integrated wearable devices (Fig. 5 and 6).[7,114] These devices require materials with high modularity, scalability, electrical conductivity, excellent fatigue resistance, electromechanical stability, a low modulus similar to human skin, and biocompatibility to improve portability and integrate seamlessly with the user's body and lifestyle, for health monitoring, human–machine interfaces, and the internet of things.[11,64,69,133] To fulfill these necessities, conductive and stretchable composites based on inorganic/organic nanomaterials have been reported, such as metal nanoparticles, nanowires, nanoribbons, nanofibers, and nanomesh (Fig. 6a and b).[134,135] The synergetic effect of metals, conductive polymers, carbon materials, and hydrogels has developed wearable and implantable sensors with promising properties.[84,109,136] For example, Namkoong *et al.*[68] fabricated a

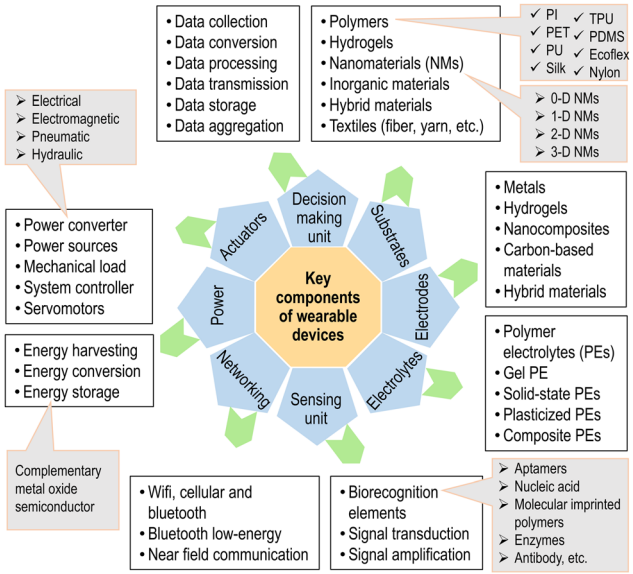

Fig. 5 Key components for assembling flexible wearable patches. Where PI, PU, and TPU are polyimide, polyurethane, and thermoplastic polyurethane, respectively.

flexible and switchable conductive nanocomposite film composed of AgNW and PEDOT/PSS using a simple and affordable micromolding technique. In addition, Zhang *et al.*[63] used a blend solution based on PDMS/PSS, water-based polyurethane, and D-sorbitol to produce flexible organic dry electrodes that enable long-term monitoring of electrophysiological signals.

However, the scalable and cost-effective development of wearable electrodes with controlled interfacial engineering between soft polymers and carbon nanomaterials remains a challenge.[19,138–140] Various fabrication techniques have been developed to create skin-like wearable materials through vacuum deposition, lithography, etching, transfer printing, the 'cut-and-paste' method, laser patterning, screen printing, inject printing, and direct skin drawing.[65,71,141] For example, Kim *et al.*[142] reported three types of biocompatible nanocomposites such as (i) PDMS/SWCNT (2 wt%), which exhibits an uneven and rough surface morphology (due to the clustering effect of SWCNT in the growth state and the presence of randomly entangled aggregate structures) and contact resistance of 1871 Ω, (ii) PDMS/SWCNT (1 wt%)/r-GO (1 wt%), exhibits uniform surface properties and low contact resistance of 63 Ω, and (iii) PDMS/SWCNT (1 wt%)/r-GO (1 wt%)/fabric, which possesses a more tightly and uniformly bonded structure, resulting in a long and wide conductive path and a significant reduction in contact resistance (15 Ω). These three types improve the resistivity of conductive and electrical properties of materials, the third electrode made from optimized nanocomposite showed comparable or superior performance to commercial Ag/AgCl gel electrodes.[143]

However, most stretchable electronic materials and devices still have elastic moduli orders of magnitude higher than soft biological tissues, limiting their applicability. Meanwhile, Li *et al.*[8] presented stretchable transistor arrays and active-matrix circuits *via* a soft interlayer design strategy with modules of less

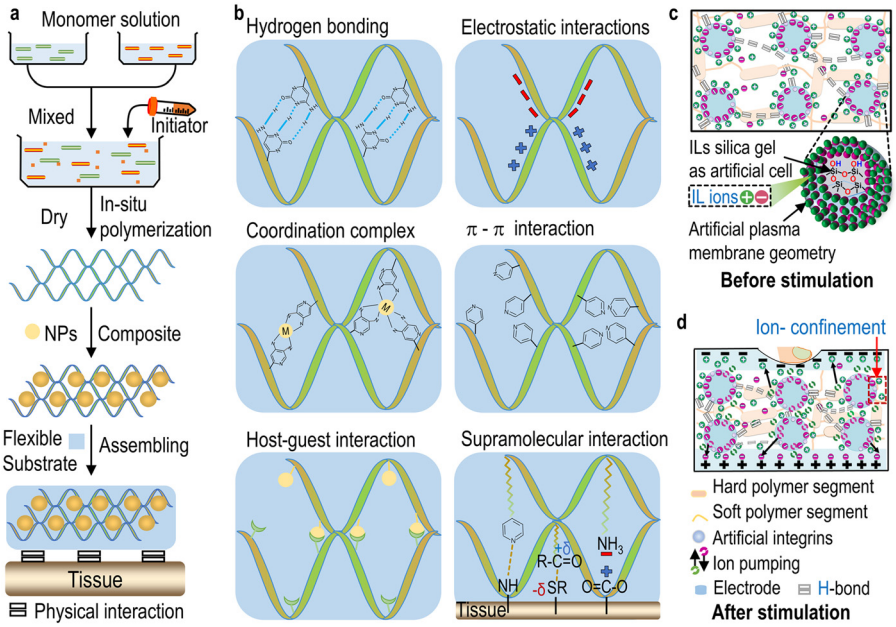

Fig. 6 Designing strategy and common cross-linking of patch-to-skin interface. (a) Fabrication process of flexible and wearable devices through polymerization. (b) The most common type of cross-linking patch-to-skin interface. (c) Building skin-like synthetic multicellular hybrid ion pump (SMHIP) containing ionic liquids (ILs, cation–anion pairs) confined in a silica microstructure (silanol groups) on the surface. (d) Ionic mechanoreceptor skin (IMS) engages in hydrogen bond-triggered reversible pumping of ions under external stimulus. (c) and (d) are reproduced from ref. 137 with permission from Springer Nature, copyright 2019.

than 10 kPa, more than two orders of magnitude lower than the current state-of-the-art.[21] In addition, Qin *et al.*[144] fabricated high-performance flexible pressure sensors using a new class of graphene-like 2D transition metal–carbon (nitrogen) compounds (MXene) with polyvinylpyrrolidone (PVP) through the laser ablation process,[145] which have outstanding features, including high sensitivity ($\sim$1.25 kPa^{-1}), low detection limit ($\sim$0.6 Pa), wide detection range (up to 294 kPa), fast response and recovery time ($\sim$30/15 ms), and mechanical stability of over 10 000 cycles.[144,146] To improve the sensitivity, the sensor's elastic modulus can be further reduced, which can be determined using eqn (1):

$$C = \frac{\varepsilon_0 \varepsilon_r A}{d} \quad (1)$$

where C represents the capacitance, ε_0 is the vacuum permittivity, ε_r is the relative permittivity, A represents the area facing the upper and lower electrodes, and d represents the distance between the electrodes.[147] In addition, the sensitivity, S of the capacitive sensor is determined as in eqn (2):

$$S = \frac{(C - C_0)/C_0}{\Delta P} = \frac{\Delta C/C_0}{\Delta P} \quad (2)$$

C is the instantaneous capacitance under load, C_0 is the initial capacitance (load-free), and ΔP is the change in applied pressure.

Furthermore, Shi *et al.*[148] developed a flexible crack-based strain sensor with improved surface adhesion and cycling durability, containing different flexible substrates (latex, PDMS, Ecoflex, and TPU).[149] These substrate modification materials (mercapto-modified, double bonds, and epoxy functional groups) all have surface adhesion (lap-shear) strength $\tau > 130$ kPa with a conductive layer including bovine serum albumin (BSA), conductive nanofillers (carbon black, CNT), PEDOT:PSS, GO, and/or MXene with a strong $\tau > 100$ kPa, and multifunctional polymers (BSA, gelatin methacryloyl (GelMA), and tetra-poly(ethylene glycol diacrylate) (tetra-PEGDA)).[150,151] As a result, the MXene/BSA-SH sensor exhibits strong surface adhesion through chemical bonds, making it resistant to peeling by 3 M tape. On the other hand, artificial skin technology uses deformable ionic materials, including ILs, ionogels, and hydrogels, to create an interface that closely resembles human skin in terms of tactile perception.[152,153]

Amoli *et al.*[137] have designed a synthetic multicellular hybrid ion pump that mimics biological cell structures, consisting of hydrogen-bonded-1-ethyl-3-methylimidazoliumbis(trifluoromethylsulfonyl)imide [EMIM$^+$][TFSI$^-$] ion pairs on the surface of silica microstructures integrated into the TPU elastic matrix. Fig. 6c illustrates that ion mechanoreceptors enable the reversible ion pumping triggered by hydrogen bonding in response to external stimuli. The resulting ion-mechanical skin is ultra-sensitive (5.77–48.1 kPa^{-1}) over a wide pressure range (0–135 kPa) at an extremely low voltage of 1 mV. It surpasses the pressure-sensing ability of natural skin mechanoreceptors such as Merkel cells, Meissner corpuscles, and Pacinian corpuscles.[154] Fig. 6d shows the design of a pressure-sensitive and piezoelectric ionic mechanical skin, with a synthetic multicellular hybrid ion pump (SMHIP) structure consisting of [EMIM$^+$][TFSI$^-$] ion pairs confined to the surface of silica microstructures embedded in TPU. This arrangement mimics the structure of an artificial plasma membrane, where

$TFSI^-$ anionic layers attach to the surface of silica microspheres through H-bonding with silanol groups. Surrounding these anions are $EMIM^+$ cations, which are attracted to the anions *via* Coulomb bonding and π–π stacking interactions of the imidazolium rings. This interaction mimics biological integrins, which are proteins involved in cell-extracellular matrix (ECM) adhesion, facilitating the rapid transmission of mechanical stimuli from the ECM to the cell. The SHMIP IL-silica-TPU membrane acts as the pressure-sensing matrix, sandwiched between deformable AgNW/PDMS electrodes that stimulate the top layer of human skin.[155–158]

3. Interaction of wearable patch-to-skin interfaces

There has been significant interest in studying skin interaction and the interface with flexible wearable devices for precisely monitoring physiological signals (Fig. 7a).[48] Various theoretical, computational, and experimental models have been used to study biomechanics, cosmetics, clinical research, and consumer goods in understanding the interaction and friction properties of human skin, as well as their practical applications.[70,72,159,160] Physical skin models such as surrogate skin (Lorica soft) and dermis equivalent test the properties of skin materials.[161] In addition, the effects of adhesion on skin friction were studied using skin slices, and the friction properties of synthetic and biological alternatives were compared.[162] Due to the complex nature of human skin, including factors such as metabolism, excretion, body temperature, and moisture, it is difficult to fully characterize these properties through isolated studies of skin friction or skin equivalent. Furthermore, current advanced technologies require bioelectronic components that adhere to the skin or are connected wirelessly to external hardware to perform tasks such as data collection, processing, and storage functionalities.[52,132,163,164]

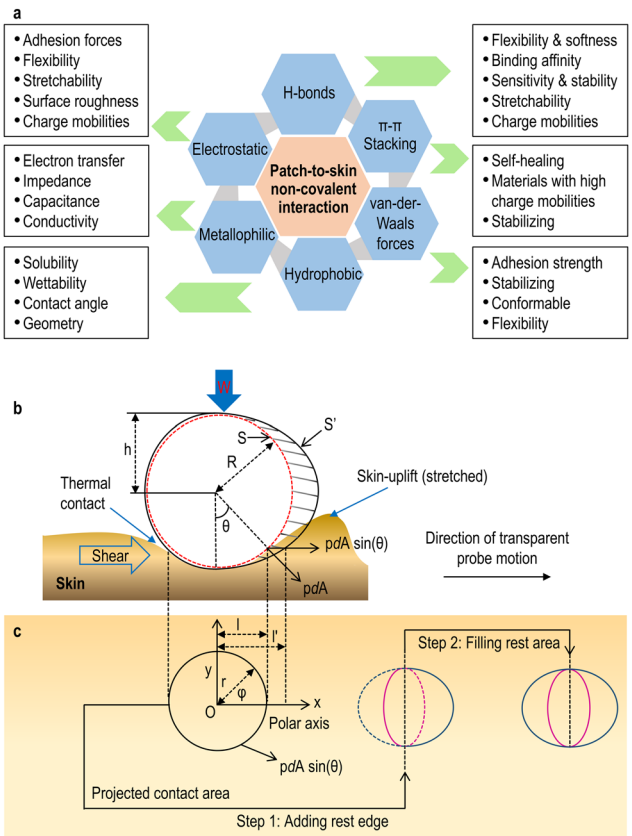

Fig. 7 Patch-to-skin non-covalent interactions and morphological coordinate system. (a) Types of non-covalent interactions between skin and wearable devices. (b) Morphology of the skin contact edge under normal contact S' (red elliptical curve) and horizontal sliding S' (black elliptical curve). (c) Deformation of the skin during sliding friction and the modeling process using a double ellipse model, where r is the perpendicular distance between any point in the contact region and the vertical line passing through the center of the sphere O, p is the contact pressure, W is the normal load, A is the contact area, R is the probe radius, and l and l' are the radii of the contact (*i.e.*, a function of W and R).

Greenwood[165] reported friction experiments on rubber and found that the uplift resistance was due to the geometric stress caused by lifting the skin, preventing the probe from sliding. They proposed a model to calculate the resistance produced by elastic deformation. In the case of low and high interfacial adhesion, local deformation can occur, which mainly leads to friction losses due to the rubber deformation. In such cases, the friction between hard spherical or conical sliders and the rubber would be higher for rubbers with low Young's moduli and larger hysteresis loss. Guan *et al.*[166] used a non-invasive method to conduct *in vivo* skin friction experiments. They observed that lifting the skin before the probe during friction tests involved horizontal movements.

The geometrical morphology of the contact area was represented by combining two elliptical models, as shown in Fig. 7b. The optical system uses the Greenwood model to project the contact morphology of the skin and provide characteristic accuracy of skin deformation. This model applies to small and large deformations and separates adhesion friction from deformation friction based on the ratio between indentation depth and probe radius. In Fig. 7c, the first step is to establish symmetrical boundaries for both the left half region (purple solid line and black dotted line) and the right half region (black solid line and purple dotted line). The next step is to fill the symmetrical region by converting the dotted lines to solid lines. This configuration allows for the use of a standard elliptical model to fit the data, as S' shown in Fig. 7b.

The contact morphology shows symmetry with the x-axis during the horizontal movement phase. Before mounting, the length equal to half the axis of the ellipse (represented by the red curve in Fig. 7b) is assumed, while h is determined by measuring half the distance between the two y-axis intersections and the contact limit. The remaining half-axis length l is adjusted accordingly. However, the small strain assumption may not be applicable due to the different indentation depths in the experiments. In light of these challenges, a model was created to determine lift-off resistance, taking into account the expected contact morphology and the hyperelastic properties of human skin. The lifting resistance model was constructed in the

polar coordinate system through coordinate transformations. Eqn (3) and (4) express the total uplift resistance:

$$F = 2\int_0^{\frac{\pi}{2}}\int_s^{s'} pr\frac{R}{\sqrt{R^2 - r^2}}\frac{r}{R}\cos\phi \mathrm{d}r\mathrm{d}\phi = \int_0^{\frac{\pi}{2}}\int_s^{s'}\frac{2pr^2\cos\phi}{\sqrt{R^2 - r^2}}\mathrm{d}r\mathrm{d}\phi \quad (3)$$

$$s = ab/\sqrt{a^2\cos^2\phi + b^2\sin^2\phi} \quad \text{and}$$
$$s' = a'b/\sqrt{b^2\cos^2\phi + a'^2\sin^2\phi} \quad (4)$$

The total horizontal resistance taking into account both lifting resistance and adhesive friction can be calculated using the equation $F_{tot} = F_{adh} - F$, where F, F_{adh}, and F_{tot} represent lifting resistance force, adhesion friction force, and experimental horizontal resistance force. However, human skin has non-ideal elastic properties (*e.g.*, hysteresis), which causes a difference between the loading and unloading curves during the elastic recovery process. Therefore, the skin cannot transfer the same amount of elastic work as observed or expected during horizontal sliding, resulting in a loss of energy that must be compensated for by frictional work. The deformation friction F_{def} can be calculated using eqn (5):

$$F_{def} = \alpha F = \alpha\int_0^{\frac{\pi}{2}}\int_s^{s'}\frac{2pr^2\cos\phi}{\sqrt{R^2 - r^2}}\mathrm{d}r\mathrm{d}\phi \quad (5)$$

where α represents the proportion of the component in the overall elastic work, expressed as a fraction of the elastic loss.

Friction properties are influenced by both contact force and contact area, in which the indentation depth increases by the expansion of the contact area, thus amplifying the adhesive component of friction, *i.e.*, a larger indentation depth corresponds to a larger degree of deformation. Moreover, the detection of sliding friction is often overlooked, and advanced techniques are lacking due to the limited understanding of surface sliding. While conventional force detection is related to tactile perception, sensing sliding friction is crucial for detecting slides, categorizing materials, and recognizing surface roughness during sliding interactions. Overall, the detection of sliding friction relies mainly on sensor networks that map pressure changes to estimate object movement.[167] However, this approach is limited when the object partially slips from the sensor array or when the size of the object is smaller than that of the sensor array. These limitations hinder the widespread application of sliding friction force in tactile interaction.[168,169]

3.1. Non-invasive chemical bioadhesive interfaces

Non-invasive chemical bioadhesive materials that can form strong bonds with biological tissues or surfaces without requiring invasive procedures are desired, relying instead on chemical interactions (Fig. 8a and b). Developing these interfaces offers benefits such as minimal tissue damage, reduced pain, improved patient comfort, and biocompatibility. These materials have the potential to revolutionize medical treatments, drug delivery systems, wound healing, and related fields by providing effective and practical solutions.[4,170] While some chemical adhesives have commonly been used to enhance the surface adhesion of sensors,

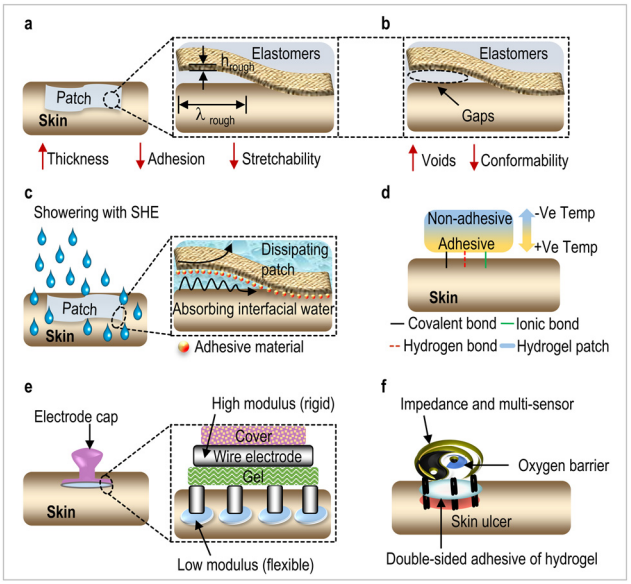

Fig. 8 Various adhesion properties of hydrogel patches for skin interfaces. (a) Stretchable hybrid wearable electrodes (SHE) exhibit soft and adhesive properties for direct skin application. The inset shows the mechanics of the skin–electrode interface during conformal contact. (b) Improper patch contact with voids. (c) Water effect on SHE adhesion, leading to weaker contact. (d) Temperature's effect, with decreasing temperatures reducing adhesion. (e) Dry adhesive electrodes supported by a hydrogel layer ensure skin–patch contact. (f) The role of hydrogel in the presence of a skin ulcer, designed to measure $tcPO_2$ and local tissue impedance.

they can often lead to skin allergies or damage and are vulnerable to moisture in wet environments. For example, a dehydrated hydrogel loses its softness, stretchability, and shape, implying that additional seals or chemicals are needed to prevent water loss.[33] Thus, electronic components must have strong adhesion properties to adhere to the skin in both dry and wet conditions while avoiding non-chemical contamination of the applied surface.[63,171] Chun *et al.*[67] improved the adhesion properties of graphene-coated fabrics (GCFs) by integrating octopus-like patterns (Ops), allowing the GCFs to maintain their strong adhesion in both dry and humid environments without extra chemicals. In dry conditions, the Ops added suction stress to the van der Waals force, while in wet environments, suction stress and capillary force were dominant. GCFs with Ops exhibited higher normal adhesion force than GCFs without Ops in both dry and wet conditions (high sensitivity at a fine pressure range <1 kPa). This indicates that GCF with Ops can be effectively used in developing waterproof wearable sensors and electrode systems that easily adhere to human skin (Fig. 8c).[171]

Additionally, polymer-ionic liquid gels (PIL gels) provide another viable option for flexible ionic conductors. Ionic liquids (ILs), which are salts with low melting points, provide a non-volatile solution at room temperature, solving the freezing and dehydration problems encountered with hydrogels in electrode-to-skin interfaces. Therefore, PIL gels exhibit improved stability compared to hydrogels, and their utility in a wide range of iontronic devices has been verified. However, the high cost and toxicity of synthetic ILs pose significant challenges to the

commercialization and transdermal applications of PIL gels.[61,172] Lim *et al.*[173] developed a skin–device interface with tissue-like properties for bioanalysis and transdermal therapy using ultrathin (~150 μm) poly(acrylamide) (PAAM) hydrogel film that provides extremely suitable contact with human skin (*i.e.*, no air gap at the surface/interface) due to their intrinsic softness (Young's modulus of polyimide (PI), PAAM hydrogel, and human skin: 2.5 GPa, 8 kPa, and 50–150 kPa, respectively).[85] This hydrogel film forms a stable, water-retaining, semi-solid surface between the wearable bioelectronic device and the human skin. When the human skin temperature reaches ~43 °C, oxygen molecules are released from the blood vessels (Fig. 8d).[174] These oxygen molecules diffuse outward from the heated skin surface and must pass through the hydrogel layer to reach the electrode (Fig. 8e). The hydrogel facilitates both heat and mass transfer, accurately sensing transcutaneous oxygen tension ($tcPO_2$) by diffusing oxygen, which is electrochemically reduced on the working electrode (maximum oxygen reduction peak in CV is near −0.7 V).[175] Surface temperatures were monitored using an infrared camera. The devices are coated with a multi-layer oxygen barrier film to prevent oxygen exchange between the device and the external environment (*e.g.*, PI/Al/PI, PEDOT/PSS/PAAM, *etc.*) (Fig. 8f). This covering layer (encapsulation) not only limits oxygen flow but also protects the hydrogel from drying out, thereby maintaining the electrochemical performance of the hydrogel electrode surface.

3.2. Non-invasive mechanical bioadhesive interfaces

Mechanical adhesion plays a key role in the connection between bioelectronics and skin interfaces. This adhesion is influenced by various factors such as geometry, humidity, viscosity, surface tension, gas counter pressure, size, thickness, weight, stretch, and softness. For instance, when a low-viscosity adhesive is applied to the surface of the skin, it forms a mechanical anchor between components such as electrodes, hydrogels, and the skin itself. Surface roughness can improve adhesion strength by increasing surface contact area; however, excessive roughness can reduce adhesion strength due to stress peaks, cavities, and fewer contact points, which limits the long-term biocompatibility of the material.[176,177] Given the growing demand for more biocompatible and less skin-irritating alternatives, dry adhesive patches offer notable advantages over acrylic polymer-based adhesives. They exhibit reproducible and reversible adhesion and are less affected by surface contamination and environmental factors such as water (Fig. 8c).[171,178] To overcome these limitations, Bae *et al.*[92] introduced a dry skin patch with enhanced adhesion, using synthetic micropillars. The base of these pillars is made from a rigid material such as hard PDMS (Young's modulus ~8.2 MPa) with a higher curing agent content, while the upper layer consists of flexible PDMS with a lower amount of curing agent (Young's modulus ~0.8 MPa) (Fig. 8e).[178,179] This synergetic combination enables the creation of monolithic integrated composite PDMS micropillars with improved strength, adhesion, and durability. The lower region acts as a stabilizer, while the tip layer ensures effective contact with human skin. The tip of the composite micropillar has a relatively low modulus, which facilitates uniform contact on rough skin surfaces. The roughness of the skin can be modeled as an array of spherical caps according to eqn (6) (where h is the height, r is the radius, and λ is the separation distance between the caps). The elastic deformation of the tip layer can be calculated by analyzing the contact between a spherical cap and the flat tip of a spatula, as shown in eqn (7). The radius of the contact area can be determined by algebraic manipulation of a unit cell.[180,181]

$$h = r - \sqrt{r^2 - \frac{\lambda^2}{4}} \tag{6}$$

$$a_{\mathrm{JKR}} = \left(\sqrt{\frac{9\pi w r^2}{8E}} + \sqrt{\frac{3\left(F + \frac{3}{2}\pi w r\right) r}{4E}} \right)^{\frac{2}{3}} \tag{7}$$

where w, F, and E represent the work of adhesion, preload, and elastic modulus, respectively. A lower modulus increases the contact area, and composite micropillars with low-modulus spatulas exhibit a greater adhesion force compared to homogeneous micropillars.

In addition, Kim *et al.*[64] developed a method to combine miniaturized electronic packages with ultra-thin connectivity platforms to enhance signal processing and long-range Bluetooth connectivity. The wireless and stretchable hybrid electronics (SHE) eliminate the need for conductive gels and adhesives. For instance, thin Au/PI electrodes (1.2 μm thick) arranged in a stretchable mesh layout can conform to complex skin structures and adapt to tissue movements, reducing film thickness to improve skin contact (Fig. 8a and b).[182] The main elastomer, ~500 μm thick, helps maintain the integrity of the electrodes during application and recovery. However, practical applications of these designs have been limited due to the fragility of the ultra-thin films upon removal and difficulties connecting them to rigid electronic packages.[183]

Moreover, increased substrate thickness can affect signal exposure, quality, and accuracy in physiological monitoring, especially when considering skin roughness (λ_{rough} and h_{rough}). Proper contact is achieved when the adhesion energy exceeds the combined elastic energy of the skin and the bending energy of the electrode. Adhesion is determined by the elastomer's work of adhesion ($\gamma_{\mathrm{elastomer}}$) and the contact surface, while elastic energy depends on the skin modulus (E_{skin}) and λ_{rough}.[184] The correlation between $\gamma_{\mathrm{elastomer}}$ and $E_{\mathrm{elastomer}}$ required for proper electrode contact assumes that onboard electronics are mechanically separated from the underlying electrodes and bonded due to the presence of a thick and flexible elastic layer. The adhesion energy ($\gamma_{\mathrm{elastomer}}$) is calculated by eqn (8), with α representing the real fraction of PI and Au.[114]

$$\gamma_{\mathrm{elastomer}} = \left(\frac{1}{1-\alpha}\right) \frac{\frac{\pi^4 E I h^2}{{\lambda_{\mathrm{rough}}}^4} + \frac{\pi E_{\mathrm{skin}}\left(h_{\mathrm{rough}} - h\right)}{16\lambda_{\mathrm{rough}}}}{1 + \frac{\pi^2 h^2}{4{\lambda_{\mathrm{rough}}}^2}} \quad \text{where} \tag{8}$$

$$h = \frac{E_{\mathrm{skin}} h_{\mathrm{rough}}}{\frac{16\pi^3 E I}{{\lambda_{\mathrm{rough}}}^3} + E_{\mathrm{skin}}}$$

In general, since animal skin differs significantly from human skin, incorporating medical films with adhesive properties like Tegaderm can provide a secure and reliable way to hold devices in place, regardless of skin condition or the activity level of the subject.[182]

3.3. Non-invasive electrical bioadhesive interfaces

The integration of bioelectronic devices with skin tissue has traditionally involved physical attachment or surgical suturing, but these methods often lead to issues such as poor contact, unstable fixation, tissue damage, and potential scarring.[4,16] Conductive polymer hydrogels have emerged as promising tissue-interfacing electrodes due to their soft, tissue-like mechanical properties. However, a trade-off between mechanical strength and electrical performance has hindered the development of hydrogels that are both tough and highly conductive, limiting their application in bioelectronics.[185] Cai *et al.*[186] addressed this issue by developing a locally coupled electromechanical interface known as CoupOn, a four-layered ionotronic assembly that mimics the cytoadhesion architecture of transmembrane proteins. The CoupOn interface achieves strong interlayer adhesion ($\sim$400 N m^{-1}) and better stability in bioelectronic applications. In contrast, a thin elastomer with dual metal nanofilms, though thinner ($\sim$40 μm compared to $\sim$140 μm for CoupOn), exhibited poor contact with the skin, indicating that surface smoothness and adhesion play a more crucial role than film thickness in achieving stable contact.[183] However, the correlation between mechanical events like muscle contraction and EMG stimulation may vary depending on factors such as muscle type and contraction force,[187,188] which complicates real-time prosthetic control. Existing methods for prosthetic control, based on strain sensors, face challenges like electromechanical delay,[189] limited sensitivity to the hand gesture,[190] inability to detect strength levels,[191] and reduced useability for amputees.

Current challenges in integrating bioelectrical devices with wet and dynamic tissues stem from poor adhesion, low conductivity, and high impedance.[192,193] For instance, dry e-bioadhesive interfaces, such as those incorporating a thin nanocomposite graphene layer, help mitigate these issues by facilitating water removal from the tissue surface through hydration and subsequent swelling in the thickness direction. This allows the interface to quickly establish a secure connection with tissue in $<$5 s, exhibiting robust interfacial toughness ($>$400 J m^{-2}) and high electrical conductivity ($>$2.6 S m^{-1}), which surpasses that of biological tissues (0.3–0.7 S m^{-1}). In general, e-bioadhesive interfaces can be engineered to maintain high water content, tissue-like softness, anisotropic swelling, and strong adhesion while remaining electrically conductive.[194,195] For example, the NHS ester groups in the e-bioadhesive interface form covalent bonds with primary amine groups on tissue surfaces, enabling a permanent bond, even under wet conditions. These bonds can be easily reversed within 5 minutes using a biocompatible solution, ensuring trauma-free device removal.[196] Additionally, the anisotropic swelling of the interface minimizes misalignment or delamination between the device and tissue in wet environments.

3.4. Non-invasive biocompatible adhesive interface

Evaluating biocompatibility typically involves tests for cytotoxicity, skin irritation, and local tissue reactivity.[197] Skin irritation tests, for example, assess both the safety and comfort of the device on the skin. In non-invasive electrode–skin interfaces, maintaining low contact impedance is essential to optimize signal quality and reduce energy loss. Enhancing electrode and material designs can improve the contact impedance between the electrode and the skin, which is critical for both user health and the functionality of medical devices and biosensors. Xue *et al.*[198] reported conductive nanocomposite hydrogel tapes (Electro-Ox hydrogel tapes), which, when applied to the bare skin of a Japanese white rabbit, showed no signs of redness, swelling, discharge, or infection. These hydrogel tapes exhibited strong adhesion ($\sim$1268 J m^{-2}) within hours of covalent bond formation. They proved effective as tissue sealants and adhesives for wearable devices and implants, even on dynamic and bleeding tissue surfaces.

Cytotoxicity and skin irritation tests further confirmed the hydrogel electrodes' excellent biocompatibility, indicating they are safe for the user's skin.[33] For instance, Deng *et al.*[4] evaluated the biocompatibility of an e-bioadhesive interface through both *in vitro* and *in vivo* testing in a mouse model. The *in vitro* cytotoxicity results were comparable to those of the control group, while the *in vivo* stability of the interface's mechanical and electrical properties was assessed by measuring conductivity, impedance, and surface strength between two gold electrodes over 14 days of implantation in a mouse subcutaneous pocket. No significant differences were observed ($P > 0.05$), demonstrating the interface's good biocompatibility. Wang *et al.*[199] developed a biocompatible conductive biogel that can be applied to the skin, which transitions reversibly between a liquid and a viscoelastic gel state depending on temperature. This gel can be easily removed with water, solving the challenge of long-term reliable EEG recording where interfaces must ensure dependable electrode contact, even with a hairy scalp.[200] Dense hair can hinder solid-like interfaces from effectively contacting the scalp, making sophisticated structural designs (*e.g.*, columnar or claw-like features) critical for consistent contact.[201] Furthermore, electrode materials must be easily removed without causing skin damage once their designated service life ends.[63,77]

4. Challenges and future directions

In the past decade, significant advances in biointerfaces have enhanced real-time health monitoring, revolutionizing biomedical applications. However, critical technological challenges remain in flexible and wearable skin interfaces. These difficulties hinder the widespread adoption of high-performance bioelectronics that integrate with human skin, particularly for applications involving dynamic tissues. Additionally, effective collecting and analyzing physiological, chemical, and electrophysiological signals requires addressing mechanical imbalances, weak adhesion forces, and electrical instability, especially in wet environments common in long-term bioelectrical systems. Improving

flexibility, stretchability, power supply integration, and protection against electrical leakage remains essential. While research on flexible batteries is ongoing, their current mechanical and electrical properties do not yet meet the needs of energy-intensive wearable and implantable bioelectronic systems. Battery-free alternatives (*e.g.*, capacitive coupling interfaces) show promise but are currently limited in their channel count and data transfer capabilities, leading to increased interference, lower signal sensitivity, and occasional device failure.

Recent data revealed that material selection, substrate pre-deformation, and device structure are crucial in manufacturing flexible wearables suitable for wet and dry environments. Addressing these issues is critical for optimizing biocompatibility, performance, and usability at the electrode–skin interface. Even small fluctuations can disrupt the balance at the skin's surface, potentially compromising signal interpretation. Wireless skin-integrated tactile interfaces, though limited by sensory feedback and operating frequency, offer potential applications in remote robot control and medicine. Approaches such as advanced discrimination tests, the integration of multiplexers, and system-on-chip designs (where key electronic components are combined on a single chip) can help overcome these limitations. Exploring haptic interfaces may also broaden interactions with the skin, including detecting surface and shear vibrations, static displacements, and thermal changes. This could lead to haptic information channels in emerging technologies like virtual reality and enhance human–machine interfaces, a promising area for future research.

Therefore, key considerations and future research directions can be summarized below: (1) material selection: devices should be designed according to the specific nature of the skin surface (smooth, rough, hairy, ulcerated, *etc.*) and its location (flat, curved, *etc.*). (2) Theoretical and computational models: While promising models exist, further experimental studies are necessary to achieve biomedical advancements (*e.g.*, hybrid energy harvesting) (3) environmental conditions: internal body conditions and external factors (*e.g.*, temperature, pressure) should be considered before application. (4) Gel-free advanced materials: these materials are needed for intelligent skin tissue regeneration. (5) Stability and scalability: ensuring material stability, biodegradability, and scalability is essential for commercialization and improving long-term signal monitoring and reliability.

5. Conclusions

In summary, biointerface sensing has emerged as a transformative approach for numerous advanced applications, including continuous health monitoring, interventional therapies, physiological, biochemical, and electrophysiological sensing, as well as tissue engineering. This technology involves intricate interactions with biological components such as cells, tissues, and organs. Wearable devices are engineered to maintain close contact with the human body, extract precise information, and influence tissue function through electrical stimulation and visible signals. Achieving an optimal balance between adhesion, mechanical strength, conductivity, and biocompatibility is essential for high sensitivity in acquiring electrophysiological signals. The thickness and Young's modulus of the substrate and electrode materials play a crucial role in determining the bending stiffness of wearable electrodes, which need to be flexible and smooth for effective contact with skin patches. In addition, the development of stretchable electronics opens up new applications for advanced ultra-flexible energy harvesting and storage solutions.[202] In fact, there are various power sources such as mechanical, thermal, chemical, solar energy, *etc.*[203] Among them, energy harvesting systems suitable for collecting different forms of energy have gained attention. For example, triboelectricity is generated during the contact-separation process of two different materials; piezoelectricity is produced during the mechanical deformation of piezoelectric materials; and electromagnetic energy is generated from a conductor moving in a steady magnetic field.[204] In all cases of the transduction mechanisms, mechanical energy is converted into electrical energy. For instance, Yu *et al.*[205] presented an ultra-soft polymeric substrate with cross-dimensional nanomaterial integration, the highly efficient and stable nanoengineered lactate biofuel cells array, which is a battery-free, fully perspiration-powered electronic skin that harvests energy from human sweat through it, performs continuous multiplexed monitoring of key metabolic biomarkers and wirelessly transmits the personalized information to a user interface *via* Bluetooth low-energy.

Deformation friction contributes minimally to total friction, with its behavior positively correlated to specific experimental conditions. Accurate assessment of shear friction requires the use of a hyperelastic model to calculate lifting resistance based on the expected contact area. One of the key limitations of flexible and stretchable electronic components in wearable biomedical devices is their inability to store recorded data in memory modules for long-term continuous monitoring. This shortcoming affects their capacity to deliver advanced therapeutic interventions based on diagnostic patterns identified from collected data. Conductive polymer hydrogels and their hybrids with nanomaterials and organic electrochemical transistors,[1] with their suitable elastic modulus, strong adhesion, excellent electrical conductivity, and biocompatibility, offer a promising solution for the next generation of human–machine interfaces. Therefore, further studying the interactions between electrodes and skin tissue is critical for understanding various human activities and improving device performance. Interdisciplinary research into electrode–skin interfaces seeks to enhance the safety, longevity, and functionality of human–machine interactions, paving the way for the seamless integration of bioelectronics into everyday life.

Author contributions

A. N. Belay drafted the manuscript; R. Guo, P. A. Koudakan, and S. Pan reviewed and edited the manuscript. S. P. provided guidance and supervision throughout the work. All authors have approved the manuscript.

Data availability

The authors declare that all relevant data presented in this review paper are available within the manuscript, and there is no supplementary information file. The source data underlying all Fig. 1–8 and Tables 1–3 are provided as source data files. No primary research results, software, or code have been included and no new data were generated or analyzed as part of this review.

Conflicts of interest

The authors declare no conflict of interest.

Acknowledgements

This work was supported by the National Natural Science Foundation of China (S. P., Grant No. 22378105 and 23FAA02526), Hunan Provincial Science and Technology Department (S. P., Project No. 2022TP2032), China Changsha Science and Technology Bureau (S. P., Project No. kq2208015), and the Australian Synchrotron, part of the Australian Nuclear Science and Technology Organization.

References

1 D. Liu, X. Tian, J. Bai, S. Wang, S. Dai, Y. Wang, Z. Wang and S. Zhang, *Nat. Electron.*, 2024, **7**, 1176–1185.
2 D. Zhong, C. Wu, Y. Jiang, Y. Yuan, M. Kim, Y. Nishio, C.-C. Shih, W. Wang, J.-C. Lai, X. Ji, T. Z. Gao, Y.-X. Wang, C. Xu, Y. Zheng, Z. Yu, H. Gong, N. Matsuhisa, C. Zhao, Y. Lei, D. Liu, S. Zhang, Y. Ochiai, S. Liu, S. Wei, J. B.-H. Tok and Z. Bao, *Nature*, 2024, **627**, 313–320.
3 Y. Shao, J. Yan, Y. Zhi, C. Li, Q. Li, K. Wang, R. Xia, X. Xiang, L. Liu, G. Chen, H. Zhang, D. Cai, H. Wang, X. Cheng, C. Yang, F. Ren and Y. Yu, *Nat. Commun.*, 2024, **15**, 6106.
4 J. Deng, H. Yuk, J. Wu, C. E. Varela, X. Chen, E. T. Roche, C. F. Guo and X. Zhao, *Nat. Mater.*, 2021, **20**, 229–236.
5 M. Bariya, H. Y. Y. Nyein and A. Javey, *Nat. Electron.*, 2018, **1**, 160–171.
6 A. Sheng, L. Lin, J. Zhu, J. Zhuang, J. Li, L. Chang and H. Cheng, *Microsyst. Nanoeng.*, 2021, **7**, 1–19.
7 J. Park, J. Kim, S. Y. Kim, W. H. Cheong, J. Jang, Y. G. Park, K. Na, Y. T. Kim, J. H. Heo, C. Y. Lee, J. H. Lee, F. Bien and J. U. Park, *Sci. Adv.*, 2018, **4**, eaap9841.
8 Y. Li, N. Li, W. Liu, A. Prominski, S. Kang, Y. Dai, Y. Liu, H. Hu, S. Wai, S. Dai, Z. Cheng, Q. Su, P. Cheng, C. Wei, L. Jin, J. A. Hubbell, B. Tian and S. Wang, *Nat. Commun.*, 2023, **14**, 4488.
9 C. Steiger, A. Abramson, P. Nadeau, A. P. Chandrakasan, R. Langer and G. Traverso, *Nat. Rev. Mater.*, 2019, **4**, 83–98.
10 Z. Wang, J. Luan, A. Seth, L. Liu, M. You, P. Gupta, P. Rathi, Y. Wang, S. Cao, Q. Jiang, X. Zhang, R. Gupta, Q. Zhou, J. J. Morrissey, E. L. Scheller, J. S. Rudra and S. Singamaneni, *Nat. Biomed. Eng.*, 2021, **5**, 64–76.
11 H. C. Ates, P. Q. Nguyen, L. Gonzalez-Macia, E. Morales-Narváez, F. Güder, J. J. Collins and C. Dincer, *Nat. Rev. Mater.*, 2022, **7**, 887–907.
12 G. Balakrishnan, J. Song, C. Mou and C. J. Bettinger, *Adv. Mater.*, 2022, **34**, 202106787.
13 I. You, D. G. MacKanic, N. Matsuhisa, J. Kang, J. Kwon, L. Beker, J. Mun, W. Suh, T. Y. Kim, J. B. H. Tok, Z. Bao and U. Jeong, *Science*, 2020, **370**, 961–965.
14 W. Guo, Y. Hu, Z. Yin and H. Wu, *Adv. Mater. Technol.*, 2022, **7**, 1–12.
15 D. Jung, C. Lim, H. J. Shim, Y. Kim, C. Park, J. Jung, S. I. Han, S. H. Sunwoo, K. W. Cho, G. D. Cha, D. C. Kim, J. H. Koo, J. H. Kim, T. Hyeon and D. H. Kim, *Science*, 2021, **373**, 1022–1026.
16 P. Tan, H. Wang, F. Xiao, X. Lu, W. Shang, X. Deng, H. Song, Z. Xu, J. Cao, T. Gan, B. Wang and X. Zhou, *Nat. Commun.*, 2022, **13**, 358.
17 E. Song, J. Li, S. M. Won, W. Bai and J. A. Rogers, *Nat. Mater.*, 2020, **19**, 590–603.
18 R. Feiner and T. Dvir, *Nat. Rev. Mater.*, 2018, **3**, 17076.
19 T. R. Ray, J. Choi, A. J. Bandodkar, S. Krishnan, P. Gutruf, L. Tian, R. Ghaffari and J. A. Rogers, *Chem. Rev.*, 2019, **119**, 5461–5533.
20 N. Davis, J. Heikenfeld, C. Milla and A. Javey, *Nat. Biotechnol.*, 2024, **42**, 860–871.
21 R. Wei, H. Li, Z. Chen, Q. Hua, G. Shen and K. Jiang, *npj Flexible Electron.*, 2024, **8**, 83.
22 N. Brasier, J. Wang, W. Gao, J. R. Sempionatto, C. Dincer, H. C. Ates, F. Güder, S. Olenik, I. Schauwecker, D. Schaffarczyk, E. Vayena, N. Ritz, M. Weisser, S. Mtenga, R. Ghaffari, J. A. Rogers and J. Goldhahn, *Nature*, 2024, **636**, 57–68.
23 R. Elnathan, M. G. Barbato, X. Guo, A. Mariano, Z. Wang, F. Santoro, P. Shi, N. H. Voelcker, X. Xie, J. L. Young, Y. Zhao, W. Zhao and C. Chiappini, *Nat. Rev. Mater.*, 2022, **7**, 953–973.
24 R. Herbert, H. Lim, B. Rigo and W. Yeo, *Sci. Adv.*, 2022, **8**, eabm1175.
25 S. Cho, H. Han, H. Park, S. U. Lee, J. H. Kim, S. W. Jeon, M. Wang, R. Avila, Z. Xi, K. Ko, M. Park, J. Lee, M. Choi, J. S. Lee, W. G. Min, B. J. Lee, S. Lee, J. Choi, J. Gu, J. Park, M. S. Kim, J. Ahn, O. Gul, C. Han, G. Lee, S. Kim, K. Kim, J. Kim, C. M. Kang, J. Koo, S. S. Kwak, S. Kim, D. Y. Choi, S. Jeon, H. J. Sung, Y. B. Park, M. Je, Y. T. Cho, Y. S. Oh and I. Park, *npj Flexible Electron.*, 2023, **7**, 8.
26 T. Kim, A. H. Kalhori, T. H. Kim, C. Bao and W. S. Kim, *Microsyst. Nanoeng.*, 2022, **8**, 120.
27 Y. He, D. Wu, M. Zhou, Y. Zheng, T. Wang, C. Lu, L. Zhang, H. Liu and C. Liu, *ACS Appl. Mater. Interfaces*, 2021, **13**, 15572–15583.
28 S. Nakata, M. Shiomi, Y. Fujita, T. Arie, S. Akita and K. Takei, *Nat. Electron.*, 2018, **1**, 596–603.
29 L. Lipani, B. G. R. Dupont, F. Doungmene, F. Marken, R. M. Tyrrell, R. H. Guy and A. Ilie, *Nat. Nanotechnol.*, 2018, **13**, 504–511.
30 P. Dongiovanni, M. Meroni, S. Casati, R. Goldoni, D. V. Thomaz, M. Del Fabbro and G. M. Tartaglia, *Int. J. Oral Sci.*, 2023, **15**, 1–12.
31 P. P. Samant, M. M. Niedzwiecki, N. Raviele, V. Tran, J. Mena-Lapaix, D. I. Walker, E. I. Felner, D. P. Jones, G. W. Miller and M. R. Prausnitz, *Sci. Transl. Med.*, 2020, **12**, 1–16.
32 S. Nakata, T. Arie, S. Akita and K. Takei, *ACS Sens.*, 2017, **2**, 443–448.
33 H. Xue, D. Wang, M. Jin, H. Gao, X. Wang, L. Xia, D. Li, K. Sun, H. Wang, X. Dong, C. Zhang, F. Cong and J. Lin, *Microsyst. Nanoeng.*, 2023, **9**, 79.
34 F. Zhang, L. Zhang, J. Xia, W. Zhao, S. Dong, Z. Ye, G. Pan, J. Luo and S. Zhang, *Adv. Sci.*, 2023, **10**, 1–10.
35 L. Yin, Y. Wang, J. Zhan, Y. Bai, C. Hou, J. Wu, R. Huang, Y. Wang and Y. A. Huang, *npj Flexible Electron.*, 2022, **6**, 29.
36 D. Kim, J. Bang, P. Won, Y. Kim, J. Jung, J. Lee, J. Kwon, H. Lee, S. Hong, N. L. Jeon, S. Han and S. H. Ko, *Adv. Mater. Technol.*, 2020, **5**, 1–8.
37 Y. Zhang, Z. Huo, X. Wang, X. Han, W. Wu, B. Wan, H. Wang, J. Zhai, J. Tao, C. Pan and Z. L. Wang, *Nat. Commun.*, 2020, **11**, 5629.
38 Y. Liang, W. Fu, Q. Li, X. Chen, H. Sun, L. Wang, L. Jin, W. Huang and B. O. Guan, *Nat. Commun.*, 2022, **13**, 7604.
39 H. Jinno, T. Yokota, M. Koizumi, W. Yukita, M. Saito, I. Osaka, K. Fukuda and T. Someya, *Nat. Commun.*, 2021, **12**, 2234.
40 H. Jang, K. Sel, E. Kim, S. Kim, X. Yang, S. Kang, K. H. Ha, R. Wang, Y. Rao, R. Jafari and N. Lu, *Nat. Commun.*, 2022, **13**, 6604.
41 N. Zavanelli, H. Kim, J. Kim, R. Herbert, M. Mahmood, Y. S. Kim, S. Kwon, N. B. Bolus, F. B. Torstrick, C. S. D. Lee and W. H. Yeo, *Sci. Adv.*, 2021, **7**, eabl4146.
42 M. Wang, Y. Yang, J. Min, Y. Song, J. Tu, D. Mukasa, C. Ye, C. Xu, N. Heflin, J. S. McCune, T. K. Hsiai, Z. Li and W. Gao, *Nat. Biomed. Eng.*, 2022, **6**, 1225–1235.
43 P. Zhu, H. Du, X. Hou, P. Lu, L. Wang, J. Huang, N. Bai, Z. Wu, N. X. Fang and C. F. Guo, *Nat. Commun.*, 2021, **12**, 4731.
44 T. Chang, H. Li, N. Zhang, X. Jiang, X. Yu, Q. Yang, Z. Jin, H. Meng and L. Chang, *Microsyst. Nanoeng.*, 2022, **8**, 25.
45 Y. Wang, L. Yin, Y. Bai, S. Liu, L. Wang, Y. Zhou, C. Hou, Z. Yang, H. Wu, J. Ma, Y. Shen, P. Deng, S. Zhang, T. Duan, Z. Li, J. Ren, L. Xiao, Z. Yin, N. Lu and Y. A. Huang, *Sci. Adv.*, 2020, **6**, eabd0996.
46 J. Lee, S. Pak, Y. W. Lee, Y. Cho, J. Hong, P. Giraud, H. S. Shin, S. M. Morris, J. I. Sohn, S. N. Cha and J. M. Kim, *Nat. Commun.*, 2017, **8**, 14734.

47 D. Akinwande and D. Kireev, *Nature*, 2019, **576**, 220–221.
48 A. Zavareh, B. Tran, C. Orred, S. Rhodes, M. S. Rahman, M. Namkoong, R. Lee, C. Carlisle, M. Rosas, A. Pavlov, I. Chen, G. Schilling, M. Smith, F. Masood, J. Hanks and L. Tian, *Adv. Mater. Technol.*, 2023, 2300206.
49 Y. Chen, Y. Zhang, Z. Liang, Y. Cao, Z. Han and X. Feng, *npj Flexible Electron.*, 2020, **4**, 2.
50 Q. Zhang, M. Xu, L. Zhou, S. Liu, W. Wang, L. Zhang, W. Xie and C. Yu, *Nat. Commun.*, 2023, **14**, 1257.
51 X. Wu, S. Wang, W. Huang, Y. Dong, Z. Wang and W. Huang, *Nat. Commun.*, 2023, **14**, 468.
52 S. Gong, X. Zhang, X. A. Nguyen, Q. Shi, F. Lin, S. Chauhan, Z. Ge and W. Cheng, *Nat. Nanotechnol.*, 2023, **18**, 889–897.
53 S. Zhu, B. Sun, G. Zhou, T. Guo, C. Ke, Y. Chen, F. Yang, Y. Zhang, J. Shao and Y. Zhao, *ACS Appl. Mater. Interfaces*, 2023, **15**, 5420–5431.
54 W. Zu, Y. Ohm, M. R. Carneiro, M. Vinciguerra, M. Tavakoli and C. Majidi, *Adv. Mater. Technol.*, 2022, **7**, 1–7.
55 A. J. Bandodkar, S. P. Lee, I. Huang, W. Li, S. Wang, C. J. Su, W. J. Jeang, T. Hang, S. Mehta, N. Nyberg, P. Gutruf, J. Choi, J. Koo, J. T. Reeder, R. Tseng, R. Ghaffari and J. A. Rogers, *Nat. Electron.*, 2020, **3**, 554–562.
56 X. Yan, X. Liu, C. Zhao and G. Q. Chen, *Signal Transduction Targeted Ther.*, 2023, **8**, 199.
57 H. Hu, Y. Ma, X. Gao, D. Song, M. Li, H. Huang, X. Qian, R. Wu, K. Shi, H. Ding, M. Lin, X. Chen, W. Zhao, B. Qi, S. Zhou, R. Chen, Y. Gu, Y. Chen, Y. Lei, C. Wang, C. Wang, Y. Tong, H. Cui, A. Abdal, Y. Zhu, X. Tian, Z. Chen, C. Lu, X. Yang, J. Mu, Z. Lou, M. Eghtedari, Q. Zhou, A. Oberai and S. Xu, *Nat. Biomed. Eng.*, 2023, **7**, 1321–1334.
58 T. Stieglitz, C. Gueli, J. Martens, N. Floto, M. Eickenscheidt, M. Sporer and M. Ortmanns, *Microsyst. Nanoeng.*, 2023, **9**, 54.
59 J. Li, Z. Liu, Y. Tang, J. Xian, C. He, H. Wu, M. Liu and F. Li, *CCS Chem.*, 2023, **5**, 1–15.
60 X. Li, Y. Song, G. Xiao, E. He, J. Xie, Y. Dai, Y. Xing, Y. Wang, Y. Wang, S. Xu, M. Wang, T. H. Tao and X. Cai, *ACS Appl. Bio Mater.*, 2021, **4**, 8013–8022.
61 G. Li, Z. Deng, M. Cai, K. Huang, M. Guo, P. Zhang, X. Hou, Y. Zhang, Y. Wang, Y. Wang, X. Wu and C. F. Guo, *npj Flexible Electron.*, 2021, **5**, 23.
62 Y. Zhao, S. Zhang, T. Yu, Y. Zhang, G. Ye, H. Cui, C. He, W. Jiang, Y. Zhai, C. Lu, X. Gu and N. Liu, *Nat. Commun.*, 2021, **12**, 4880.
63 L. Zhang, K. S. Kumar, H. He, C. J. Cai, X. He, H. Gao, S. Yue, C. Li, R. C. S. Seet, H. Ren and J. Ouyang, *Nat. Commun.*, 2020, **11**, 4683.
64 Y. S. Kim, M. Mahmood, Y. Lee, N. K. Kim, S. Kwon, R. Herbert, D. Kim, H. C. Cho and W. H. Yeo, *Adv. Sci.*, 2019, **6**, 1900939.
65 A. Zahed, H. Yoon, D. K. Kim, S. Jeong, G. B. Pradhan, Y. Do Shin, S. H. Yoon, S. Sharma, S. Zhang and J. Y. Park, *Adv. Funct. Mater.*, 2022, **32**, 2208344.
66 S. Zhang, A. Chhetry, M. A. Zahed, S. Sharma, C. Park, S. Yoon and J. Y. Park, *npj Flexible Electron.*, 2022, **6**, 11.
67 S. Chun, W. Son, D. W. Kim, J. Lee, H. Min, H. Jung, D. Kwon, A. H. Kim, Y. J. Kim, S. K. Lim, C. Pang and C. Choi, *ACS Appl. Mater. Interfaces*, 2019, **11**, 16951–16957.
68 M. Namkoong, H. Guo, M. S. Rahman, D. Wang, C. J. Pfeil, S. Hager and L. Tian, *npj Flexible Electron.*, 2022, **6**, 41.
69 H. U. Chung, B. H. Kim, J. Y. Lee, J. Lee, Z. Xie, E. M. Ibler, K. H. Lee, A. Banks, J. Y. Jeong, J. Kim, C. Ogle, D. Grande, Y. Yu, H. Jang, P. Assem, D. Ryu, J. W. Kwak, M. Namkoong, J. Bin Park, Y. Lee, D. H. Kim, A. Ryu, J. Jeong, K. You, B. Ji, Z. Liu, Q. Huo, X. Feng, Y. Deng, Y. Xu, K. I. Jang, J. Kim, Y. Zhang, R. Ghaffari, C. M. Rand, M. Schau, A. Hamvas, D. E. Weese-Mayer, Y. Huang, S. M. Lee, C. H. Lee, N. R. Shanbhag, A. S. Paller, S. Xu and J. A. Rogers, *Science*, 2019, **363**, 1–13.
70 S. Burattini, B. W. Greenland, D. H. Merino, W. Weng, J. Seppala, H. M. Colquhoun, W. Hayes, M. E. MacKay, I. W. Hamley and S. J. Rowan, *J. Am. Chem. Soc.*, 2010, **132**, 12051–12058.
71 F. Ershad, A. Thukral, J. Yue, P. Comeaux, Y. Lu, H. Shim, K. Sim, N. I. Kim, Z. Rao, R. Guevara, L. Contreras, F. Pan, Y. Zhang, Y. S. Guan, P. Yang, X. Wang, P. Wang, X. Wu and C. Yu, *Nat. Commun.*, 2020, **11**, 3823.
72 S. Zhang, A. Chhetry, M. A. Zahed, S. Sharma, C. Park, S. Yoon and J. Y. Park, *npj Flexible Electron.*, 2022, **6**, 11.
73 J. Jung, S. Lee, H. Kim, W. Lee, J. Chong, I. You and J. Kang, *Nat. Commun.*, 2024, **15**, 9763.
74 H. Ye, B. Wu, S. Sun and P. Wu, *Nat. Commun.*, 2024, **15**, 885.
75 G. Wang, E. Sweren, W. Andrews, Y. Li, J. Chen, Y. Xue, E. Wier, M. P. Alphonse, L. Luo, Y. Miao, R. Chen, D. Zeng, S. Lee, A. Li, E. Dare, D. Kim, N. K. Archer, S. K. Reddy, L. Resar, Z. Hu, E. A. Grice, M. A. Kane and L. A. Garza, *Sci. Adv.*, 2023, **9**, eabo7555.
76 N. Tiwari, E. R. Osorio-Blanco, A. Sonzogni, D. Esporrín-Ubieto, H. Wang and M. Calderón, *Angew. Chem.*, 2022, **134**, 202107960.
77 S. Chen, L. Sun, X. Zhou, Y. Guo, J. Song, S. Qian, Z. Liu, Q. Guan, E. Meade Jeffries, W. Liu, Y. Wang, C. He and Z. You, *Nat. Commun.*, 2020, **11**, 1107.
78 W. Zhang, B. Wu, S. Sun and P. Wu, *Nat. Commun.*, 2021, **12**, 4082.
79 T. Sun, F. Tasnim, R. T. Mcintosh, N. Amiri, D. Solav, M. T. Anbarani, D. Sadat, L. Zhang, Y. Gu, M. A. Karami and C. Dagdeviren, *Nat. Biomed. Eng.*, 2020, **4**, 954–972.
80 T. Someya and M. Amagai, *Nat. Biotechnol.*, 2019, **37**, 382–388.
81 J. Yang, Z. Zhang, P. Zhou, Y. Zhang, Y. Liu, Y. Xu, Y. Gu, S. Qin, H. Haick and Y. Wang, *Nanoscale*, 2023, **15**, 3051–3078.
82 Z. Wang, H. Bai, W. Yu, Z. Gao, W. Chen, Z. Yang, C. Zhu, Y. Huang, F. Lv and S. Wang, *Sci. Adv.*, 2022, **8**, eabo1458.
83 J. Kim, P. Kantharaju, H. Yi, M. Jacobson, H. Jeong, H. Kim, J. Lee, J. Matthews, N. Zavanelli, H. Kim, H. Jeong, M. Kim and W. H. Yeo, *npj Flexible Electron.*, 2023, **7**, 3.
84 Y. T. Kwon, Y. S. Kim, S. Kwon, M. Mahmood, H. R. Lim, S. W. Park, S. O. Kang, J. J. Choi, R. Herbert, Y. C. Jang, Y. H. Choa and W. H. Yeo, *Nat. Commun.*, 2020, **11**, 3450.
85 C. Lim, Y. J. Hong, J. Jung, Y. Shin, S. H. Sunwoo, S. Baik, O. K. Park, S. H. Choi, T. Hyeon, J. H. Kim, S. Lee and D. H. Kim, *Sci. Adv.*, 2021, **7**, eabd3716.
86 X. Xiong, Y. Chen, Z. Wang, H. Liu, M. Le, C. Lin, G. Wu, L. Wang, X. Shi, Y. G. Jia and Y. Zhao, *Nat. Commun.*, 2023, **14**, 1331.
87 Z. Zhu, R. Li and T. Pan, *Adv. Mater.*, 2018, **30**, 1705122.
88 K. Lee, X. Ni, J. Y. Lee, H. Arafa, D. J. Pe, S. Xu, R. Avila, M. Irie, J. H. Lee, R. L. Easterlin, D. H. Kim, H. U. Chung, O. O. Olabisi, S. Getaneh, E. Chung, M. Hill, J. Bell, H. Jang, C. Liu, J. Bin Park, J. Kim, S. B. Kim, S. Mehta, M. Pharr, A. Tzavelis, J. T. Reeder, I. Huang, Y. Deng, Z. Xie, C. R. Davies, Y. Huang and J. A. Rogers, *Nat. Biomed. Eng.*, 2020, **4**, 148–158.
89 N. Xia, D. Jin, C. Pan, J. Zhang, Z. Yang, L. Su, J. Zhao, L. Wang and L. Zhang, *Nat. Commun.*, 2022, **13**, 7514.
90 D. Y. Khang, J. A. Rogers and H. H. Lee, *Adv. Funct. Mater.*, 2009, **19**, 1526–1536.
91 Q. Liu, J. Huang, J. Zhang, Y. Hong, Y. Wan, Q. Wang, M. Gong, Z. Wu and C. F. Guo, *ACS Appl. Mater. Interfaces*, 2018, **10**, 2026–2032.
92 W. G. Bae, D. Kim, M. K. Kwak, L. Ha, S. M. Kang and K. Y. Suh, *Adv. Healthcare Mater.*, 2012, **2**, 109–113.
93 Y. H. Jung, J. Yoo, A. Vázquez-guardado, J. Kim, J. Kim, H. Luan, M. Park, J. Lim, H. Shin, C. Su, R. Schloen, J. Trueb, R. Avila, J. Chang, D. S. Yang, Y. Park, H. Ryu, H. Yoon, G. Lee, H. Jeong, J. U. Kim, A. Akhtar, J. Cornman, T. Kim, Y. Huang and J. A. Rogers, *Nat. Electron.*, 2022, **5**, 374–385.
94 X. Xia, X. Zhang, M. J. Serpe and Q. Zhang, *Adv. Mater. Technol.*, 2019, 1900818.
95 D. H. Kim, N. Lu, R. Ma, Y. S. Kim, R. H. Kim, S. Wang, J. Wu, S. M. Won, H. Tao, A. Islam, K. J. Yu, T. Il Kim, R. Chowdhury, M. Ying, L. Xu, M. Li, H. J. Chung, H. Keum, M. McCormick, P. Liu, Y. W. Zhang, F. G. Omenetto, Y. Huang, T. Coleman and J. A. Rogers, *Science*, 2011, **333**, 838–843.
96 H. Y. Y. Nyein, M. Bariya, B. Tran, C. H. Ahn, B. J. Brown, W. Ji, N. Davis and A. Javey, *Nat. Commun.*, 2021, **12**, 1823.
97 L. B. Baker, *Temperature*, 2019, **6**, 211–259.
98 J. V. Vaghasiya, C. C. Mayorga-Martinez, J. Vyskočil and M. Pumera, *Nat. Commun.*, 2023, **14**, 2.
99 Y. J. Wang, X. N. Zhang, Y. Song, Y. Zhao, L. Chen, F. Su, L. Li, Z. L. Wu and Q. Zheng, *Chem. Mater.*, 2019, **31**, 1430–1440.
100 C. Wang, P. Zhang, W. Xiao, J. Zhao, M. Shi, H. Wei, Z. Deng, B. Guo, Z. Zheng and Y. Yu, *Nat. Commun.*, 2020, **11**, 4694.
101 X. Ming, L. Yao, H. Zhu, Q. Zhang and S. Zhu, *Adv. Funct. Mater.*, 2022, **32**, 2109850.
102 X. Xu, Y. L. Eatmon, K. S. S. Christie, A. L. McGaughey, N. Guillomaitre, S. S. Datta, Z. J. Ren, C. Arnold and R. D. Priestley, *JACS Au*, 2023, **3**, 2772–2779.
103 A. F. da Silva, A. F. Moreira, S. P. Miguel and P. Coutinho, *Adv. Colloid Interface Sci.*, 2024, **333**, 103297.
104 J. Li, Z. Liu, Y. Tang, J. Xian, C. He, H. Wu, M. Liu and F. Li, *CCS Chem.*, 2023, **5**, 1–15.

105 N. Cohen, C. Du and Z. L. Wu, *Macromolecules*, 2021, **54**, 11316–11325.
106 S. Wu, M. Hua, Y. Alsaid, Y. Du, Y. Ma, Y. Zhao, C. Lo, C. Wang, D. Wu, B. Yao, J. Strzalka, H. Zhou, X. Zhu and X. He, *Adv. Mater.*, 2021, **33**, 2007829.
107 Z. Li, D. Wang, H. Bai, S. Zhang, P. Ma and W. Dong, *Macromol. Mater. Eng.*, 2019, **305**, 1900623.
108 J. H. Ha, Y. Jeong, J. Ahn, S. Hwang, S. Jeon, D. Kim, J. Ko, B. Kang, Y. Jung, J. Choi, H. Han, J. Gu, S. Cho, H. Kim, M. Bok, S. A. Park, J. H. Jeong and I. Park, *Mater. Horiz.*, 2023, **10**, 4163–4171.
109 Q. Liang, X. Xia, X. Sun, D. Yu, X. Huang, G. Han, S. M. Mugo, W. Chen and Q. Zhang, *Adv. Sci.*, 2022, **9**, 2201059.
110 X. Yu, Z. Xie, Y. Yu, J. Lee, A. Vazquez-guardado, H. Luan, J. Ruban, X. Ning, A. Akhtar, D. Li, B. Ji, Y. Liu, R. Sun, J. Cao, Q. Huo, Y. Zhong, C. Lee, S. Kim, P. Gutruf, C. Zhang, Y. Xue, Q. Guo, A. Chempakasseril, P. Tian, W. Lu, J. Jeong, Y. Yu, J. Cornman, C. Tan, B. Kim, K. Lee, X. Feng, Y. Huang and J. A. Rogers, *Nature*, 2019, **575**, 473–479.
111 Y. Huang, J. Zhou, P. Ke, X. Guo, C. K. Yiu, K. Yao, S. Cai, D. Li, Y. Zhou, J. Li, T. H. Wong, Y. Liu, L. Li, Y. Gao, X. Huang, H. Li, J. Li, B. Zhang, Z. Chen, H. Zheng, X. Yang, H. Gao, Z. Zhao, E. Song, H. Wu, Z. Wang, Z. Xie, K. Zhu and X. Yu, *Nat. Electron.*, 2023, **6**, 1020–1031.
112 C. Dhong, R. Miller, N. B. Root, S. Gupta, L. V. Kayser, C. W. Carpenter, K. J. Loh, V. S. Ramachandran and D. J. Lipomi, *Sci. Adv.*, 2019, **5**, eaaw8845.
113 M. Zhu, Z. Sun, Z. Zhang, Q. Shi, T. He, H. Liu, T. Chen and C. Lee, *Sci. Adv.*, 2020, **6**, eaaz8693.
114 M. Carlotti, V. Mattoli, A. Mazzotta and V. Mattoli, *Mater. Adv.*, 2021, **2**, 1787–1820.
115 D. Li, J. He, Z. Song, K. Yao, M. Wu, H. Fu, Y. Liu, Z. Gao, J. Zhou, L. Wei, Z. Zhang, Y. Dai, Z. Xie and X. Yu, *Microsyst. Nanoeng.*, 2021, **7**, 85.
116 E. Acome, S. K. Mitchell, T. G. Morrissey, M. B. Emmett, C. Benjamin, M. King, M. Radakovitz and C. Keplinger, *Science*, 2018, **359**, 61–65.
117 M. Nakajima, K. Hasegawa, Y. Makino and H. Shinoda, *IEEE Trans. Haptics*, 2021, **14**, 874–884.
118 A. Frisoli and D. Leonardis, *Nat. Rev. Electr. Eng.*, 2024, **1**, 666–679.
119 Y. Huang, J. Zhou, P. Ke, X. Guo, C. K. Yiu, K. Yao, S. Cai, D. Li, Y. Zhou, J. Li, T. H. Wong, Y. Liu, L. Li, Y. Gao, X. Huang, H. Li, J. Li, B. Zhang, Z. Chen, H. Zheng, X. Yang, H. Gao, Z. Zhao, X. Guo, E. Song, H. Wu, Z. Wang, Z. Xie, K. Zhu and X. Yu, *Nat. Electron.*, 2023, **6**, 1020–1031.
120 O. R. Bilal, V. Costanza, A. Israr, A. Palermo, P. Celli, F. Lau and C. Daraio, *Adv. Mater. Technol.*, 2020, **5**, 2000181.
121 B. Xu, A. Akhtar, Y. Liu, H. Chen, W. Yeo, S. I. I. Park, B. Boyce, H. Kim, J. Yu, H. Lai, S. Jung, Y. Zhou, J. Kim, S. Cho, Y. Huang, T. Bretl and J. A. Rogers, *Adv. Mater.*, 2016, **28**, 4462–4471.
122 E. Song, Z. Xie, W. Bai, H. Luan, B. Ji, X. Ning, Y. Xia, M. J. Baek, Y. Lee, R. Avila, H.-Y. Chen, J.-H. Kim, S. Madhvapathy, K. Yao, D. Li, J. Zhou, M. Han, S. M. Won, X. Zhang, D. J. Myers, Y. Mei, X. Guo, S. Xu, J.-K. Chang, X. Yu, Y. Huang and J. A. Rogers, *Nat. Biomed. Eng.*, 2021, **5**, 759771.
123 Y. Liu, C. Yiu, Z. Song, Y. Huang, K. Yao, T. Wong, J. Zhou, L. Zhao, X. Huang, S. K. Nejad, M. Wu, D. Li, J. He, X. Guo, J. Yu, X. Feng, Z. Xie and X. Yu, *Sci. Adv.*, 2022, **8**, eabl6700.
124 H. Bai, S. Li and R. F. Shepherd, *Adv. Funct. Mater.*, 2021, 2009364.
125 F. Mancini, A. Bauleo, J. Cole, F. Lui, C. A. Porro, P. Haggard and G. D. Iannetti, *Ann. Neurol.*, 2014, **75**, 917–924.
126 Y. H. Jung, J. Kim and J. A. Rogers, *Adv. Funct. Mater.*, 2020, **31**, 2008805.
127 Q. Van Duong, V. P. Nguyen, A. T. Luu and S. T. Choi, *Sci. Rep.*, 2019, **9**, 13290.
128 S. Zhang, R. J. Klein, K. Ren, B. Chu, X. Zhang and J. Runt, *J. Mater. Sci.*, 2006, **41**, 271–280.
129 K. Kim and J. E. Colgate, *IEEE Trans. Neural Syst. Rehabil. Eng.*, 2012, **20**, 798–805.
130 K. Yao, J. Zhou, Q. Huang, M. Wu, C. K. Yiu, J. Li, X. Huang, D. Li, J. Su, S. Hou, Y. Liu, Y. Huang, Z. Tian, J. Li, H. Li, R. Shi, B. Zhang, J. Zhu, T. H. Wong, H. Jia, Z. Gao, Y. Gao, Y. Zhou, W. Park, E. Song, M. Han, H. Zhang, J. Yu, L. Wang, W. J. Li and X. Yu, *Nat. Mach. Intell.*, 2022, **4**, 893–903.
131 C. Larson, B. Peele, S. Li, S. Robinson, M. Totaro, L. Beccai, B. Mazzolai and R. Shepherd, *Science*, 2016, **351**, 1071–1074.
132 C. Kim, H. Lee, K. H. Oh and J. Sun, *Science*, 2016, **353**, 2957–2961.
133 Y. Liu, M. Pharr and G. A. Salvatore, *ACS Nano*, 2017, **11**, 9614–9635.
134 A. Miyamoto, S. Lee, N. F. Cooray, S. Lee, M. Mori, N. Matsuhisa, H. Jin, L. Yoda, T. Yokota, A. Itoh, M. Sekino, H. Kawasaki, T. Ebihara, M. Amagai and T. Someya, *Nat. Nanotechnol.*, 2017, **12**, 907–913.
135 S. Lee, S. Franklin, F. A. Hassani, T. Yokota, M. O. G. Nayeem, Y. Wang, R. Leib, G. Cheng, D. W. Franklin and T. Someya, *Science*, 2020, **370**, 966–970.
136 Y. Yamamoto, S. Harada, D. Yamamoto, W. Honda, T. Arie, S. Akita and K. Takei, *Sci. Adv.*, 2016, **2**, e1601473.
137 V. Amoli, J. S. Kim, E. Jee, Y. S. Chung, S. Y. Kim, J. Koo, H. Choi, Y. Kim and D. H. Kim, *Nat. Commun.*, 2019, **10**, 4019.
138 M. M. Hasan and M. M. Hossain, *J. Mater. Sci.*, 2021, **56**, 14900–14942.
139 Y. Yoon, P. L. Truong, D. Lee and S. H. Ko, *ACS Nanosci. Au*, 2022, **2**, 64–92.
140 Y. Gu, Z. Qiu and K. Müllen, *J. Am. Chem. Soc.*, 2022, **144**, 11499–11524.
141 N. Li, Y. Li, Z. Cheng, Y. Liu, Y. Dai, S. Kang, S. Li, N. Shan, S. Wai, A. Ziaja, Y. Wang, J. Strzalka, W. Liu, C. Zhang, X. Gu, J. A. Hubbell, B. Tian and S. Wang, *Science*, 2023, **381**, 686–693.
142 D. Y. Kim, G. Lee, G. Y. Lee, J. Kim, K. Jeon and K. S. Kim, *Nanoscale Adv.*, 2022, **4**, 4570–4578.
143 H. Wu, G. Yang, K. Zhu, S. Liu, W. Guo, Z. Jiang and Z. Li, *Adv. Sci.*, 2021, **8**, 2001938.
144 R. Qin, M. Hu, X. Li, T. Liang, H. Tan, J. Liu and G. Shan, *Microsyst. Nanoeng.*, 2021, **7**, 100.
145 A. V. Mohammadi, J. Rosen and Y. Gogotsi, *Science*, 2021, **372**, eabf1581.
146 S. Sharma, A. Chhetry, M. Sharifuzzaman, H. Yoon and J. Y. Park, *ACS Appl. Mater. Interfaces*, 2020, **12**, 22212–22224.
147 S. R. A. Ruth, L. Beker, H. Tran, V. R. Feig, N. Matsuhisa and Z. Bao, *Adv. Funct. Mater.*, 2020, **30**, 201903100.
148 X. Shi, H. Wang, X. Xie, Q. Xue, J. Zhang, S. Kang, C. Wang, J. Liang and Y. Chen, *ACS Nano*, 2019, **13**, 649–659.
149 F. Barthelat, Z. Yin and M. J. Buehler, *Nat. Rev. Mater.*, 2016, **1**, 16007.
150 X. Shi, L. Zhu, H. Yu, Z. Tang, S. Lu, H. Yin, M. You, G. Sun and Q. Chen, *Adv. Funct. Mater.*, 2023, **33**, 2301036.
151 X. Hu, J. Tian, C. Li, H. Su, R. Qin, Y. Wang, X. Cao and P. Yang, *Adv. Mater.*, 2020, **32**, 1–11.
152 H. R. Lee, C. C. Kim and J. Y. Sun, *Adv. Mater.*, 2018, **30**, 1–15.
153 R. Yang, A. Dutta, B. Li, N. Tiwari and W. Zhang, *Nat. Commun.*, 2023, **14**, 2907.
154 M. L. Jin, S. Park, Y. Lee, J. H. Lee, J. Chung, J. S. Kim, J. S. Kim, S. Y. Kim, E. Jee, D. W. Kim, J. W. Chung, S. G. Lee, D. Choi, H. T. Jung and D. H. Kim, *Adv. Mater.*, 2017, **29**, 1–9.
155 Y. He, Q. Li, P. Chen, Q. Duan, J. Zhan, X. Cai, L. Wang, H. Hou and X. Qiu, *Nat. Commun.*, 2022, **13**, 7666.
156 L. Yu, Y. Hou, W. Xie, J. L. Cuellar-Camacho, Q. Wei and R. Haag, *Adv. Mater.*, 2020, **32**, 1–11.
157 M. S. Ganewatta, Z. Wang and C. Tang, *Nat. Rev. Chem.*, 2021, **5**, 753–772.
158 J. Y. Sun, X. Zhao, W. R. K. Illeperuma, O. Chaudhuri, K. H. Oh, D. J. Mooney, J. J. Vlassak and Z. Suo, *Nature*, 2012, **489**, 133–136.
159 H. Zahouani, C. Pailler-Mattei, B. Sohm, R. Vargiolu, V. Cenizo and R. Debret, *Sking Res. Technol.*, 2009, **15**, 68–76.
160 X. Liu, M. J. Carré, Q. Zhang, Z. Lu, S. J. Matcher and R. Lewis, *Sking Res. Technol.*, 2018, **24**, 31–44.
161 A. K. Dabrowska, G. M. Rotaru, S. Derler, F. Spano, M. Camenzind, S. Annaheim, R. Stämpfli, M. Schmid and R. M. Rossi, *Sking Res. Technol.*, 2016, **22**, 3–14.
162 S. Suhail, N. Sardashti, D. Jaiswal, S. Rudraiah, M. Misra and S. G. Kumbar, *Biotechnol. J.*, 2019, **14**, 1900022.
163 K. R. Jinkins, S. Li, H. Arafa, H. Jeong, Y. J. Lee, C. Wu, E. Campisi, X. Ni, D. Cho, Y. Huang and J. A. Rogers, *Sci. Adv.*, 2022, **8**(1), eabo053.
164 M. Kaltenbrunner, T. Sekitani, J. Reeder, T. Yokota, K. Kuribara, T. Tokuhara, M. Drack, R. Schwödiauer, I. Graz, S. Bauer-Gogonea, S. Bauer and T. Someya, *Nature*, 2013, **499**, 458–463.
165 J. A. Greenwood and D. Tabor, *Proc. Phys. Soc.*, 1958, **71**, 989–1001.
166 Z. Y. Guan, L. Zhou, L. A. Li, H. X. Wei, W. J. Chen, S. B. Wang and C. W. Li, *J. Mech. Behav. Biomed. Mater.*, 2020, **104**, 103692.
167 A. Charalambides and S. Bergbreiter, *Adv. Mater. Technol.*, 2017, **2**, 1–10.

168 Y. Li, M. Zhao, Y. Yan, L. He, Y. Wang, Z. Xiong, S. Wang, Y. Bai, F. Sun, Q. Lu, Y. Wang, T. Li and T. Zhang, *npj Flexible Electron.*, 2022, **6**, 46.
169 Z. Ren, J. Nie, J. Shao, Q. Lai, L. Wang, J. Chen, X. Chen and Z. L. Wang, *Adv. Funct. Mater.*, 2018, **28**, 201802989.
170 C. Xie, X. Wang, H. He, Y. Ding and X. Lu, *Adv. Funct. Mater.*, 2020, **30**, 201909954.
171 S. Baik, D. W. Kim, Y. Park, T. Lee, S. H. Bhang and C. Pang, *Nature*, 2017, **546**, 396–400.
172 Z. He and W. Yuan, *ACS Appl. Mater. Interfaces*, 2021, **13**, 53055–53066.
173 C. Lim, Y. Shin, J. Jung, J. H. Kim, S. Lee and D. H. Kim, *APL Mater.*, 2019, **7**, 1–11.
174 V. E. de Meijer, H. P. van't Sant, S. Spronk, F. J. Kusters and P. T. den Hoed, *J. Vasc. Surg.*, 2008, **48**, 382–388.
175 S. Iguchi, K. Mitsubayashi, T. Uehara and M. Ogawa, *Sens. Actuators, B*, 2005, **108**, 733–737.
176 V. W. Wong, K. C. Rustad, S. Akaishi, M. Sorkin, J. P. Glotzbach, M. Januszyk, E. R. Nelson, K. Levi, J. Paterno, I. N. Vial, A. A. Kuang, M. T. Longaker and G. C. Gurtner, *Nat. Med.*, 2012, **18**, 148–152.
177 L. A. Galuska, E. S. Muckley, Z. Cao, D. F. Ehlenberg, Z. Qian, S. Zhang, S. Rondeau-Gagné, M. D. Phan, J. F. Ankner, I. N. Ivanov and X. Gu, *Nat. Commun.*, 2021, **12**, 2347.
178 M. K. Kwak, H. E. Jeong and K. Y. Suh, *Adv. Mater.*, 2011, **23**, 3949–3953.
179 C. M. Stafford, C. Harrison, K. L. Beers, A. Karim, E. J. Amis, M. R. Vanlandingham, H. C. Kim, W. Volksen, R. D. Miller and E. E. Simonyi, *Nat. Mater.*, 2004, **3**, 545–550.
180 A. Bietsch and B. Michel, *J. Appl. Phys.*, 2000, **88**, 4310–4318.
181 D. Qin, Y. Xia and G. M. Whitesides, *Nat. Protoc.*, 2010, **5**, 491–502.
182 W. H. Yeo, Y. S. Kim, J. Lee, A. Ameen, L. Shi, M. Li, S. Wang, R. Ma, S. H. Jin, Z. Kang, Y. Huang and J. A. Rogers, *Adv. Mater.*, 2013, **25**, 2773–2778.
183 J. W. Jeong, W. H. Yeo, A. Akhtar, J. J. S. Norton, Y. J. Kwack, S. Li, S. Y. Jung, Y. Su, W. Lee, J. Xia, H. Cheng, Y. Huang, W. S. Choi, T. Bretl and J. A. Rogers, *Adv. Mater.*, 2013, **25**, 6839–6846.
184 S. Wang, M. Li, J. Wu, D. H. Kim, N. Lu, Y. Su, Z. Kang, Y. Huang and J. A. Rogers, *J. Appl. Mech. Trans. ASME*, 2012, **79**, 1–6.
185 J. Chong, C. Sung, K. S. Nam, T. Kang, H. Kim, H. Lee, H. Park, S. Park and J. Kang, *Nat. Commun.*, 2023, **14**, 2206.
186 P. Cai, C. Wan, L. Pan, N. Matsuhisa, K. He, Z. Cui, W. Zhang, C. Li, J. Wang, J. Yu, M. Wang, Y. Jiang, G. Chen and X. Chen, *Nat. Commun.*, 2020, **11**, 2183.
187 T. Masuda, T. Kizuka, J. Y. Zhe, H. Yamada, K. Saitou, T. Sadoyama and M. Okada, *J. Electromyogr. Kinesiol.*, 2001, **11**, 85–94.
188 Y. Jiang, Z. Liu, C. Wang and X. Chen, *Acc. Chem. Res.*, 2019, **52**, 82–90.
189 H. Begovic, G. Q. Zhou, T. Li, Y. Wang and Y. P. Zheng, *Front. Physiol.*, 2014, **5**, 1–9.
190 J. Eom, R. Jaisutti, H. Lee, W. Lee, J. S. Heo, J. Y. Lee, S. K. Park and Y. H. Kim, *ACS Appl. Mater. Interfaces*, 2017, **9**, 10190–10197.
191 K. C. Pradel, W. Wu, Y. Ding and Z. L. Wang, *Nano Lett.*, 2014, **14**, 6897–6905.
192 Q. Yang, T. Wei, R. T. Yin, M. Wu, Y. Xu, J. Koo, Y. S. Choi, Z. Xie, S. W. Chen, I. Kandela, S. Yao, Y. Deng, R. Avila, T. L. Liu, W. Bai, Y. Yang, M. Han, Q. Zhang, C. R. Haney, K. Benjamin Lee, K. Aras, T. Wang, M. H. Seo, H. Luan, S. M. Lee, A. Brikha, N. Ghoreishi-Haack, L. Tran, I. Stepien, F. Aird, E. A. Waters, X. Yu, A. Banks, G. D. Trachiotis, J. M. Torkelson, Y. Huang, Y. Kozorovitskiy, I. R. Efimov and J. A. Rogers, *Nat. Mater.*, 2021, **20**, 1559–1570.
193 P. Mao, H. Li and Z. Yu, *Sensors*, 2023, **23**, 3673.
194 C. Gabriel, A. Peyman and E. H. Grant, *Phys. Med. Biol.*, 2009, **54**, 4863–4878.
195 H. Yuk, C. E. Varela, C. S. Nabzdyk, X. Mao, R. F. Padera, E. T. Roche and X. Zhao, *Nature*, 2019, **575**, 169–174.
196 X. Chen, H. Yuk, J. Wu, C. S. Nabzdyk and X. Zhao, *Proc. Natl. Acad. Sci. U. S. A.*, 2020, **117**, 15497–15503.
197 J. Park, Y. Lee, T. Y. Kim, S. Hwang and J. Seo, *ACS Appl. Electron. Mater.*, 2022, **4**, 1449–1468.
198 B. Xue, J. Gu, L. Li, W. Yu, S. Yin, M. Qin, Q. Jiang, W. Wang and Y. Cao, *Nat. Commun.*, 2021, **12**, 7156.
199 C. Wang, H. Wang, B. Wang, H. Miyata, Y. Wang, M. O. G. Nayeem, J. J. Kim, S. Lee, T. Yokota, H. Onodera and T. Someya, *Sci. Adv.*, 2022, **8**, eabo1396.
200 G. Li, S. Wang, M. Li and Y. Y. Duan, *J. Neural Eng.*, 2021, **18**, 046016.
201 G. Shen, K. Gao, N. Zhao, Z. Yi, C. Jiang, B. Yang and J. Liu, *J. Neural Eng.*, 2021, **18**, 066047.
202 Q. Shi, T. He and C. Lee, *Nano Energy*, 2019, **57**, 851–871.
203 R. Yu, S. Feng, Q. Sun, H. Xu, Q. Jiang, J. Guo, B. Dai, D. Cui and K. Wang, *J. Nanobiotechnol.*, 2024, **22**, 497.
204 Z. Xue, Y. Gai, Y. Wu, Z. Liu and Z. Li, *Commun. Mater.*, 2024, **5**, 211.
205 Y. Yu, J. Nassar, C. Xu, J. Min, Y. Yang, A. Dai, R. Doshi, A. Huang, Y. Song, R. Gehlhar, A. D. Ames and W. Gao, *Sci. Robot.*, 2020, **5**, eaaz7946.